USE OF THE PARTICLE LEVEL SET METHOD FOR ENHANCED RESOLUTION OF FREE SURFACE FLOWS

A DISSERTATION
SUBMITTED TO THE PROGRAM IN
SCIENTIFIC COMPUTING AND COMPUTATIONAL MATHEMATICS
AND THE COMMITTEE ON GRADUATE STUDIES
OF STANFORD UNIVERSITY
IN PARTIAL FULFILLMENT OF THE REQUIREMENTS
FOR THE DEGREE OF
DOCTOR OF PHILOSOPHY

Douglas Patrick Enright
August 2002

I certify that I have read this dissertation and that, in my opinion, it is fully adequate in scope and quality as a dissertation for the degree of Doctor of Philosophy.

Ronald P. Fedkiw
(Computer Science)
(Principal Advisor)

I certify that I have read this dissertation and that, in my opinion, it is fully adequate in scope and quality as a dissertation for the degree of Doctor of Philosophy.

Joel H. Ferziger
(Mechanical Engineering)

I certify that I have read this dissertation and that, in my opinion, it is fully adequate in scope and quality as a dissertation for the degree of Doctor of Philosophy.

Juan J. Alonso
(Aeronautics and Astronautics)

Approved for the University Committee on Graduate Studies:

Abstract

A new numerical method for improving the mass conservation properties of the level set method when the interface is passively advected in a flow field is proposed. The method, a hybrid "Particle Level Set Method", uses Lagrangian marker particles to rebuild a level set representation of the interface in regions which are under-resolved. This is often the case for flows undergoing stretching and tearing. A level set only approach towards maintaining small-scale interface features is subject to excessive amounts of numerical regularization. This numerical regularization artificially alters or destroy these features. By combining a simple Lagrangian method, massless marker particles, with the level set method, the ability to smoothly represent both large and small scale geometrical features is obtained while maintaining the implementation simplicity characteristic of the level set method. A variety of interface tracking tests, including a newly proposed three dimensional deformation flow test case, are performed to demonstrate that the method compares favorably with volume of fluid methods in the conservation of mass and purely Lagrangian schemes for interface resolution.

The robustness of the method in representing complex, three dimensional free surface fluid flows is illustrated through its use in producing physically based animations of the pouring of a glass of water; the splash generated by the impact of a ball thrown into a tank of water; and the breaking of a wave on a submerged beach. The behavior of the water is calculated by a three dimensional Navier-Stokes free surface fluid simulation. A novel application of a level set based velocity extrapolation technique is used to provide a smooth, physically based velocity field away from the liquid at the interface. This velocity field satisfies the physical boundary conditions

at the interface and provides a plausible velocity field for use by Lagrangian particles outside the liquid as required by the "Particle Level Set Method". Selected frames from each of the animations are provided.

Acknowledgments

The material in this dissertation is drawn from two articles, "A Hybrid Particle Level Set Method for Improved Interface Capturing" to appear in the Journal of Computational Physics and "Animation and Rendering of Complex Water Surfaces" published in the Proceedings of SIGGRAPH 2002.

Research supported in part by an ONR YIP and PECASE award N00014-01-1-0620, the DOE ASCI Academic Strategic Alliances Program (LLNL contract B341491), NSF DMS-0106694, and a Howard Hughes Doctoral Fellowship from the Hughes Aircraft and Raytheon Systems Companies.

Contents

List of Tables

List of Figures

Chapter 1

Introduction

"It's the pouring of milk into a glass."
Jeffrey Katzenberg [33]

1.1 Background

The above response to a question concerning what was the single hardest shot in the feature film "Shrek", exemplifies the difficulty of the task that has faced the computational fluid dynamics community over the past 50 years - to accurately simulate complex, three dimensional liquid behavior. In order to obtain the degree of realism required of engineering and computer graphics applications, the nonlinear phenomena present in liquids needs to be modeled and simulated. This requires the use of a three dimensional model of the behavior of liquids, the Navier-Stokes equations, along with a moving boundary technique to handle the merging and pinching off of liquid elements. Simulating these models on a computer also requires that appropriate numerical methods are used to ensure that the results generated are faithful to nature while at the same time incorporate a variety of practical engineering needs including robustness, speed, and stability.

The need to capture complex topological features which can develop in three dimensional free surface flows is a serious constraint when considering what type of moving boundary method to use to model the free surface. Purely Lagrangian flow

models, e.g. boundary integral and vortex methods [7, 37, 36, 48, 29, 19] suffer from an inability to model changes in topology (pinching and merging) of the interface. Utilizing a fixed grid representation for the flow variables (pressure, densities, velocities, etc.) can alleviate some of the difficulties mentioned above, but we are then faced with the question of how to model the interface. A Lagrangian representation in the spirit of Tryggvason *et al.* [92, 91] via particles placed on the interface and advected by the flow can deal with arbitrary topologies, but at the cost of implementing and verifying the correctness of complex algorithms required to rearrange the connectivity of particles in order to effect changes in topology. Marker particle based methods [31, 15, 64, 16, 90] have a long history in modeling the motion of interfaces. These methods avoid the geometrical complexities of connected front tracking algorithms, but at the price of lacking a smooth, well defined interface. The interface can form gaps and holes due to a lack of marker particle in cells which should be connected. Also as noted in [15], careful consideration of the velocity boundary conditions to apply at the surface of the liquid is required in order to avoid introducing asymmetries and other computational artifacts. Finally, both methods can require the use of artificial smoothing near the interface in order to obtain smooth geometrical quantities [97].

A grid based Eulerian representation of the free surface avoids the many issues inherent to Lagrangian schemes. Both Volume of Fluid (VOF) [34, 63] and the level set method [60, 85] can easily support complex topologies. However, the use in VOF of a single variable to represent the amount of liquid in a computational cell introduces its own set of difficulties. In the attempt to maintain local mass conservation, "blobby" flotsam and jetsam can spuriously appear [45], especially in under-resolved regions of the flow due to excessive numerical surface tension being added to the simulation. Also, the reconstructed interface is not smooth or even continuous, lowering the accuracy of the geometrical information (normals and curvature) at the interface which can compromise the solution. Several researchers have worked to improve the accuracy of the VOF geometrical information using convolution, see e.g. [94] and [93].

On the other hand, the level set method use a function $\phi(\vec{x}, t)$ whose isocontour

$\phi = 0$ is used to represent the interface. This function is advected by a flow field given by $\vec{u}(\vec{x}, t)$. Mathematically, the evolution of the level set is given by

$$\phi_t + \vec{u} \cdot \nabla \phi = 0. \tag{1.1}$$

While level set methods have seen much success on a wide variety of problems including fluid mechanics, combustion, computer vision, and materials science as discussed in the recent review articles and books by Osher and Fedkiw [58, 59] and Sethian [75, 74], their application to free surface flows has been problematic. As noted in [85], the signed distance property of the initial level set function quickly ceases to exist after a couple of time steps of equation 1.1, especially on coarse computational grids. Since the interface is defined by a single isocontour of ϕ, the signed distance property away from the interface is not required. However, accurate evolution of the level set function which represents a contact discontinuity is severely impaired if the gradient of ϕ is not smooth. How the level set method deal with this issue and how to create a numerical method which corrects for this built in characteristic of the level set method, is a key issue that will be addressed in this work.

1.2 Curvature and Numerical Regularization

The great success of level set methods (and other Eulerian methods) can be attributed to the role of curvature in numerical regularization which allows the proper vanishing viscosity solution to be obtained. This regularization of the level set function allows the method to handle changes in topology in a natural manner. The connection between curvature and the notion of entropy conditions and shocks for hyperbolic conservation laws was explored by Sethian [70, 71]. No Lagrangian scheme, including discretization of the interface by marker particles, can achieve a similar result since there is no *a priori* way to build regularization into the method. Lagrangian particles faithfully follow the characteristics of the flow, but must be deleted (usually "by hand") if the characteristics merge.

The ability to identify and delete merging characteristics is clearly seen in a purely

geometrically driven flow in which a curve is advected normal to itself at constant speed. Figure 1.1 shows an initially square interface taken as the $\phi = 0$ isocontour of a level set function along with the associated velocity field defined by $\nabla\phi/|\nabla\phi|$. This flow field has merging characteristics on the diagonals of the square. Figure 1.2 shows that a numerical solution computed using the level set method correctly shrinks the box as time increases. On the other hand, a Lagrangian front tracking model of the interface will not calculate the correct motion. We demonstrate this by seeding passively advected particles interior to the zero isocontour of the level set function as shown in figure 1.3. As the particle positions evolve in time, they follow the characteristic velocities of the flow field as shown in figure 1.4. The particles incorrectly form long, slender filaments on the diagonals of the square where characteristics merge that should be deleted (as is correctly done by the level set method). Helmsen [32] and others have used "de-looping" procedures in an attempt to remove these incorrect particle tails. While these procedures are sometimes manageable in two spatial dimensions, they become intractable in three spatial dimensions.

Despite a lack of explicit enforcement of conservation, Lagrangian schemes are quite successful in conserving mass since they preserve material advected along characteristics for all time as opposed to regularizing mass out of existence as Eulerian front capturing methods may do. For under-resolved flows, Eulerian capturing methods can not accurately tell if characteristics merge, separate, or are parallel. This indeterminacy can cause level set methods to calculate weak solutions and delete characteristics when they appear to be merging. Osher and Sethian [60] constructed the level set method to deal with the case in which characteristics *do* merge as seen in figure 1.2, i.e. to recognize the presence of shocks and delete merging characteristic information. We are faced with the difficult question of the appropriateness of using level set schemes that merge characteristics automatically when we lack knowledge about the characteristic structure in under-resolved regions of the flow. Moreover, in the case of incompressible fluid flows, we know *a priori* that there are no shocks present in the velocity field, and thus characteristic information should never be deleted.

An Eulerian analysis can yield some insight into a possible solution to this problem.

If we use an upwind spatial discretization of equation 1.1 along with a first order temporal discretization, we obtain (in one spatial dimension)

$$\frac{\phi_i^{n+1} - \phi_i^n}{\Delta t} + u_i^n (D^{\pm}\phi)_i^n = 0, \tag{1.2}$$

where $D^{\pm}\phi$ is a forward/backward difference of ϕ,

$$\begin{aligned} (D^+\phi)_i^n &= \frac{\phi_{i+1}^n - \phi_i^n}{\Delta x}, \\ (D^-\phi)_i^n &= \frac{\phi_i^n - \phi_{i-1}^n}{\Delta x}. \end{aligned}$$

Which difference to take is determined by the sign of u_i^n according to the *method of characteristics*. For $u_i^n > 0$, we choose $D^-\phi$ since information is flowing from left to right and $D^+\phi$ for $u_i^n < 0$. What is of more interest is the numerical error associated with the spatial discretization of equation 1.2. To lowest order in Δx, the error term is

$$\pm\frac{\Delta x}{2}\left(\frac{\partial^2\phi}{\partial x^2}\right)_i^n + O(\Delta x^2). \tag{1.3}$$

In higher dimensions on an equally spaced grid, this error term is $\epsilon\triangle\phi$, with $\epsilon \sim \Delta x$. Since this term is an inherent part of our calculation, if we substitute the exact solution of equation 1.1, Φ, into our finite difference approximation, we obtain

$$\frac{\Phi_i^{n+1} - \Phi_i^n}{\Delta t} + u_i^n (D^{\pm}\Phi)_i^n = \pm\frac{\Delta x}{2}\left(\frac{\partial^2\Phi}{\partial x^2}\right)_i^n, \tag{1.4}$$

which is accurate to $O(\Delta x)$. As $\Delta x \to 0$, the finite difference solution $\phi_i^n \to \Phi(\vec{x}, t)$ in the sense that ϕ_i^n is a vanishing viscosity solution to equation 1.1. The smoothing viscosity-like term on the right hand side of equation 1.4 provides a way to regularize the solution obtained by the level set method in order to deal with shocks which form due to changes in the topology of the interface. However, if Δx is not sufficiently small and/or we are trying to resolve features on the order of $O(\Delta x)$, then the right hand side of equation 1.4 does not approach zero. In this case (which is unfortunately a common occurrence in many interesting interfacial flow problems) we are left with

a solution to equation 1.4, a convection-diffusion equation, rather than the solution our original advection equation. If ϕ is a signed distance function, then the diffusion present in equation 1.4 is proportional to the curvature of the interface. Regions of high curvature relative to the grid size will experience the most diffusion.

The difficulties of using the level set method to capture contact discontinuities has been brought to light by a series of test problems proposed by Rider and Kothe [67, 68]. These problems either contain large vortical flow components, inducing the formation of under-resolved regions of the interface, or the interface possesses regions of extremely high curvature, e.g. corners, which should be preserved during a rigid body movement of the interface. By comparing various Lagrangian and Eulerian methods for these flows, Rider and Kothe found that Lagrangian tracking schemes maintain filamentary interface structures better than their Eulerian counterparts. In the same study, it was noted that when fluid filaments become too thin to be adequately resolved on the grid, level set methods lose (or gain) mass while VOF methods form "blobby" filaments that locally enforce mass conservation but in the process artificially move the interface. Both types of errors decrease the accuracy of the interface location. The loss (or gain) of mass by level set methods can be attributed to the diffusion present in equation 1.4 in an Eulerian sense or the incorrect merging (or creation) of characteristics in a Lagrangian sense.

Attempts to improve mass conservation in level set methods have led to a variety of Eulerian based methods. As noted earlier, Sussman *et al.* [85] recognized this problem and proposed to reinitialize ϕ in order to maintain a smooth level set function. While this method did improve the spatial discretization properties of ϕ, it did not directly address the issue of under-resolved regions/regions of high curvature. Further improvements to this reinitialization method by Sussman and Fatemi [83, 84] include the introduction of a Lagrange multiplier constraint which attempts to preserve mass on a cell-by-cell basis. Higher order ENO/WENO [39] approximations for the spatial derivatives in the convection and reintialization steps have been proposed. Although the use of higher order spatial approximations does indeed help conserve mass, as shown in chapter 3, in regions where the level set senses that shocks are occurring and applies numerical regularization to the interface, the accuracy of the interface

decreases to first order. We are then left with situation discussed earlier. Cheng *et al.* [13], addressed the curvature-based diffusion present in level set methods through the use of an anti-diffusive reinitialization scheme. The method attempts to move the level set in a manner to recover the amount of area/volume lost during a time step. An alternative approach to reinitialization has been proposed by Adalsteinsson and Sethian [2]. In this scheme one smoothly extrapolates the velocity of the interface away from the interface and moves ϕ according to this "extension velocity". In many level set applications this is a required procedure, since no velocity exists off the interface. In the case of fluid flows however, the fluid velocity is a valid "extension velocity". However, in under-resolved regions this scheme requires the use of suspect geometrical information contained in the level set function. Finally, Sussman and Puckett [80] combined VOF and level set methods in order to alleviate some of the problems of the VOF method. The resulting scheme is completely Eulerian in nature and does not incorporate any of the front-tracked characteristic information needed in under-resolved regions. Instead, the VOF local mass constraint is still blindly applied. The level set method is only used as a smoother in order to obtain better approximations of the curvature of the interface than is possible with VOF methods. None of these methods take advantage of the underlying characteristic flow field information that Lagrangian interface methods successfully utilize.

1.3 Scope and Presentation

In this dissertation, we propose a new method which combines the best properties of an Eulerian level set method and a marker particle Lagrangian scheme. Our method randomly places a set of marker particles near the interface (defined by the zero level set) and allows them to passively advect with the flow. In fluid flows, particles do not cross the interface except when the interface capturing scheme fails to accurately identify the interface location. If marker particles initially seeded on one side of the interface are detected on the opposite side, this indicates an error in the level set representation of the interface. We fix these errors by locally rebuilding the level set function using the characteristic information present in these escaped marker

particles. This allows the level set method to obtain sub-grid scale accuracy near the interface and works to counteract the mass loss of the level set method in under-resolved regions. The particles play no other role in the calculation and the smooth geometry of the interface is determined by the level set function alone. Also, since the marker particles are treated separately, the ease and simplicity of coding level set methods is maintained by this "particle level set" method. Chapter 2 discusses the use and implementation of the "particle level set" method in more detail. Numerical results based upon two and three dimensional interface stretch tests proposed and inspired by Rider and Kothe [67, 68] are presented in chapter 3 to demonstrate that the new "particle level set" technique compares favorably with VOF methods with regard to mass conservation and with purely Lagrangian schemes with regard to interface resolution. We then utilize the "particle level set" method coupled with a novel application of the velocity extrapolation technique of Adalsteinsson and Sethian in order to obtain smooth interface behavior for a variety of three dimensional free surface calculations for computer graphics applications. The application of these techniques to animate the pouring of a glass of water, the behavior of a splash sheet formed by a ball thrown into a tank of water, and the breaking of a wave upon a beach are shown in chapter 4. Conclusions about the use of the "particle level set" method for modeling free surface flows and avenues of future research are discussed in chapter 5.

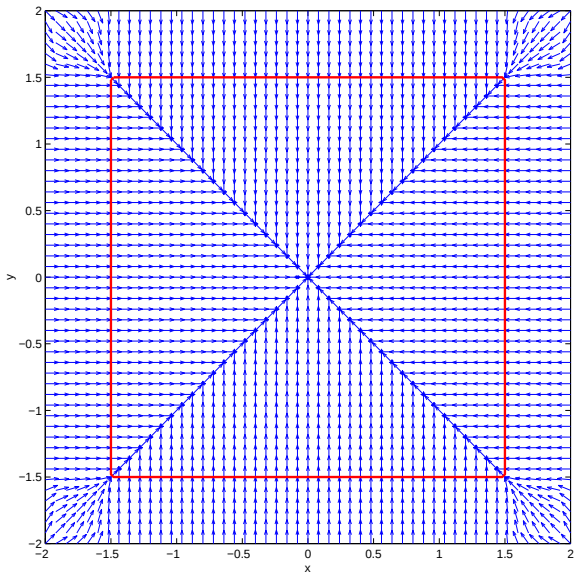

Figure 1.1: Shrinking square. Initial interface location and velocity field.

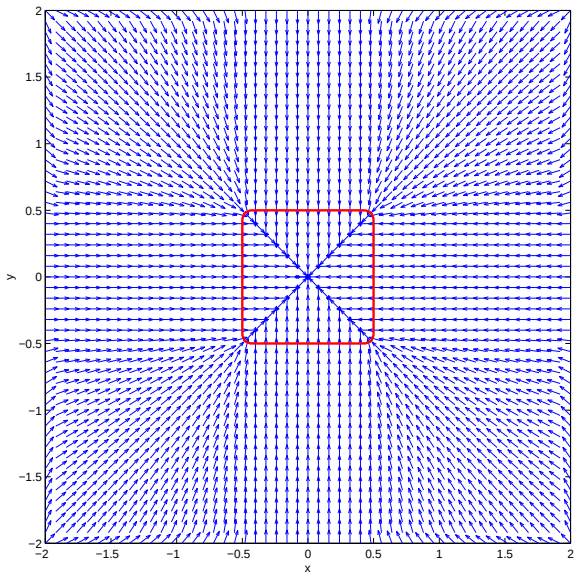

Figure 1.2: Shrinking square. Final interface location of the (correct) level set solution.

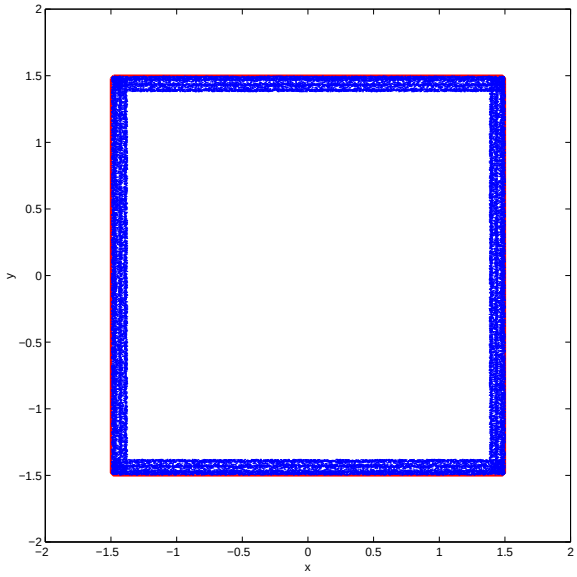

Figure 1.3: Shrinking square. Passively advected particles are initially seeded inside the interface.

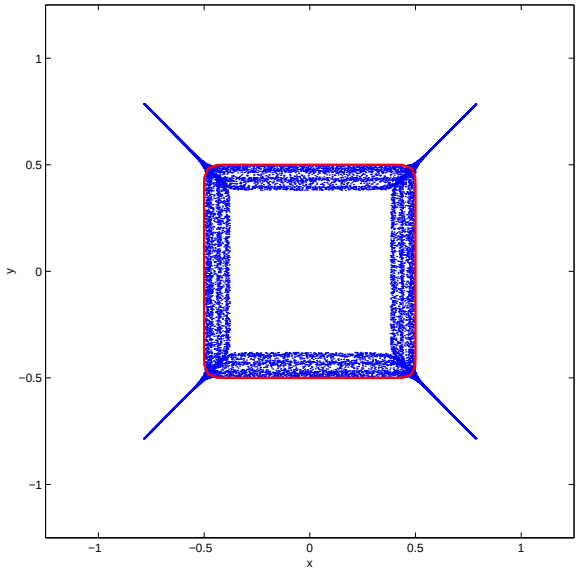

Figure 1.4: Shrinking square. Final (incorrect) location of the passively advected marker particles.

Chapter 2

Numerical Method

"I think it [interface tracking] is a subject worthy of a great deal of effort on its own; although it appears almost trivial, it really isn't, and it really ought to be done well, once and for all, if that is possible."

R. DeBar [21]

2.1 Level Set Method

The underlying idea behind level set methods is to embed an interface Γ in R^3 which bounds an open region $\Omega \subset R^3$ as the zero level set of a higher dimensional function $\phi(\vec{x}, t)$. The level set function has the following properties,

$$\begin{aligned} \phi(\vec{x}, t) &> 0 \qquad \text{for } \vec{x} \in \Omega \\ \phi(\vec{x}, t) &\leq 0 \qquad \text{for } \vec{x} \notin \Omega, \end{aligned}$$

where we include $\phi = 0$ with the negative ϕ values so that it is not a special case. The interface lies between $\phi > 0$ and $\phi = 0$, but can of course be identified as $\phi = 0$. Note that ϕ is a scalar function in R^3 which greatly reduces the complexity of describing the interface, especially when undergoing topological changes such as pinching and merging.

The motion of the interface is determined by a velocity field, $\vec{u}$, which can depend

on a variety of things including position, time, geometry of the interface, or be given externally, for instance as the material velocity in a fluid flow simulation. In most of the examples below, the velocity field is externally given, and the evolution equation for the level set function is given by

$$\phi_t + \vec{u} \cdot \nabla \phi = 0. \tag{2.1}$$

This equation only needs to be solved locally near the interface, e.g. see [1, 62].

Both ϕ and $\vec{u} = (u, v, w)$ are represented on a fixed Cartesian grid with a constant grid spacing of $\Delta x = \Delta y = \Delta z$. We use a dimension by dimension approach in discretizing $\vec{u} \cdot \nabla \phi = u\phi_x + v\phi_y + w\phi_z$ term in equation 2.1. For the sake of brevity, we proceed by discussing only the discretization of $u\phi_x$. At a specific grid point, x_i, we choose either a left-sided or right-sided discretization of ϕ_x according to the local velocity at x_i. This corresponds to discretizing equation 2.1 according to the method of characteristics. For $u_i < 0$, we take $\phi_x = \phi_x^+$ and for $u_i > 0$, we take $\phi_x = \phi_x^-$. Since level set methods appear to be sensitive to the accuracy used in discretizing the spatial derivatives, we used a fifth order accurate Hamilton-Jacobi WENO scheme [39] to calculate right and left biased derivatives, ϕ_x^+ and ϕ_x^-, needed by the method of characteristics.

To find ϕ_x^-, set

$$v_1 = \frac{\phi_{i-2} - \phi_{i-3}}{\Delta x}, \qquad v_2 = \frac{\phi_{i-1} - \phi_{i-2}}{\Delta x}$$
$$v_3 = \frac{\phi_i - \phi_{i-1}}{\Delta x}, \qquad v_4 = \frac{\phi_{i+1} - \phi_i}{\Delta x}$$
$$v_5 = \frac{\phi_{i+2} - \phi_{i+1}}{\Delta x}$$

and to find ϕ_x^+, set

$$v_1 = \frac{\phi_{i+3} - \phi_{i+2}}{\Delta x}, \qquad v_2 = \frac{\phi_{i+2} - \phi_{i+1}}{\Delta x}$$
$$v_3 = \frac{\phi_{i+1} - \phi_i}{\Delta x}, \qquad v_4 = \frac{\phi_i - \phi_{i-1}}{\Delta x}$$

$$v_5 = \frac{\phi_{i-1} - \phi_{i-2}}{\Delta x}.$$

We utilize these first order divided differences to obtain three different polynomial approximations of $\phi_x^{\pm}$,

$$\phi_x^1 = \frac{v_1}{3} - \frac{7v_2}{6} + \frac{11v_3}{6} \tag{2.2}$$

$$\phi_x^2 = \frac{-v_2}{6} + \frac{5v_3}{6} + \frac{v_4}{3} \tag{2.3}$$

$$\phi_x^3 = \frac{v_3}{3} + \frac{5v_4}{6} - \frac{v_5}{6}. \tag{2.4}$$

Essentially Non-Oscillatory (ENO) methods choose one of the above three approximations. The choice of which approximation to use is made according to which approximation generates the smoothest possible polynomial interpolation of ϕ. This choice will hopefully approximate $\phi_x^{\pm}$ with the least error. For Weighted ENO methods, a weighted convex combination of equations 2.2- 2.4 is used. The weights $w_1, w_2, \text{and } w_3$, are calculated using an estimate of the smoothness of each stencil. These smoothness estimates are given by

$$\begin{aligned} S_1 &= \frac{13}{12}(v_1 - 2v_2 + v_3)^2 + \frac{1}{4}(v_1 - 4v_2 + 3v_3)^2 \\ S_2 &= \frac{13}{12}(v_2 - 2v_3 + v_4)^2 + \frac{1}{4}(v_2 - v_4)^2 \\ S_3 &= \frac{13}{12}(v_3 - 2v_4 + v_5)^2 + \frac{1}{4}(3v_3 - 4v_4 + v_5)^2 \end{aligned}$$

and the weights by

$$\begin{aligned} a_1 &= \frac{1}{10}\frac{1}{(\epsilon + S_1)^2}, & w_1 &= \frac{a_1}{a_1 + a_2 + a_3} \\ a_2 &= \frac{6}{10}\frac{1}{(\epsilon + S_2)^2}, & w_2 &= \frac{a_2}{a_1 + a_2 + a_3} \\ a_3 &= \frac{3}{10}\frac{1}{(\epsilon + S_3)^2}, & w_3 &= \frac{a_3}{a_1 + a_2 + a_3} \end{aligned}$$

in order to obtain

$$(\phi_x^{\pm})_i = w_1(\frac{v_1}{3} - \frac{7v_2}{6} + \frac{11v_3}{6}) + w_2(\frac{-v_2}{6} + \frac{5v_3}{6} + \frac{v_4}{3}) + w_3(\frac{v_3}{3} + \frac{5v_4}{6} - \frac{v_5}{6}). \quad (2.5)$$

Note that $\epsilon = 10^{-6}$.

To integrate equation 2.1 forward in time via the method of lines, it is desirable to use a time integration scheme which does not produce any spurious oscillations, i.e. one that possesses the property of being Total Variation Diminishing (TVD). A basic first order TVD scheme is the forward Euler method. To obtain a higher-order accurate explicit Runge-Kutta TVD scheme, a convex combination of forward Euler steps may be formed with positive weights. Unfortunately, HJ WENO spatial discretization combined with upwind differencing is not TVD, but is most likely Total Variation Bounded (TVB). We choose to use a third-order TVD Runge-Kutta method as discussed in [76]. Let $E(\phi)$ represent a forward Euler update such that $\phi^{n+1} = E(\phi^n) = \phi^n + \Delta t(\vec{u}^n \cdot \nabla\phi^n)$, then a third-order Runge-Kutta method is

$$\phi^{n+1} = \frac{1}{3}\phi^n + \frac{2}{3}E(\frac{3}{4}\phi^n + \frac{1}{4}E(E(\phi^n))). \quad (2.6)$$

For the numerical test cases presented in chapter 3, only ϕ is integrated in time since we assume $\vec{u}(\vec{x}, t)$ is given at grid points.

In a level set method, it is convenient to make ϕ equal to the signed distance to the interface so that $|\nabla\phi| = 1$. This ensures that the level set is a smoothly varying function well suited for high order accurate numerical methods. Unfortunately, as noted in [85], the level set function can quickly cease to be a signed distance function especially for flows undergoing extreme topological changes. Reinitialization algorithms maintain the signed distance property by solving to steady state (as fictitious time $\tau \to \infty$) the equation

$$\phi_\tau + \mathrm{sgn}(\phi_0)(|\nabla\phi| - 1) = 0 \quad (2.7)$$

where $\text{sgn}(\phi_0)$ is a one-dimensional smeared sign function that is approximated numerically in [85] as

$$\text{sgn}(\phi_0) = \frac{\phi_0}{\sqrt{\phi_0^2 + (\Delta x)^2}}.$$

Efficient ways to solve equation 2.7 to steady state via fast marching methods are discussed in [72]. However, while it is possible to construct second order accurate marching methods as discussed in [73], these methods become increasingly problematic due to the need to use higher order accurate interpolants to initialize the function on the band of grid points surrounding the $\phi = 0$ isocontour. For the current state of the art concerning fast marching method solutions to equation 2.7 we refer the reader to [17].

For the purposes of calculating a second order accurate distance function near the interface while avoiding the computational difficulties discussed above, we perform 10 iterations of equation 2.7 in a narrow band (10 grid cells) about $\phi = 0$. At the same time we perform a first order fast marching method over the entire grid. Outside the narrow band, we use the value of ϕ calculated by the fast marching method while inside the narrow band we use the value calculated via equation 2.7 unless it differs from the fast marching solution by more than $\max(\Delta x, \Delta y, \Delta z)$. In this case, we choose the value obtained by the fast marching method. We also prevent ϕ from changing sign during the reinitialization process and use a fifth order accurate Hamilton-Jacobi WENO scheme as described above to calculate the spatial derivatives in equation 2.7.

Geometrical quantities can be calculated from the level set function, including the unit normal to the interface,

$$\vec{N} = \frac{\nabla\phi}{|\nabla\phi|}, \tag{2.8}$$

and the curvature,

$$\kappa = \nabla \cdot \left(\frac{\nabla\phi}{|\nabla\phi|} \right). \tag{2.9}$$

The spatial derivatives in equations 2.8 and 2.9 can be calculated using standard second order accurate central differencing when the denominators are non-zero. When $|\nabla\phi| = 0$ one-sided differencing is used.

2.2 Massless Marker Particles

Two sets of massless but finite size marker particles are placed near the interface with one set, the *positive* particles, in the $\phi > 0$ region and the other set, the *negative* particles, in the $\phi \leq 0$ region. It is unnecessary to place particles far from the interface since the sign of the level set function easily identifies these regions. This greatly reduces the number of particles needed in a simulation. Traditional marker particle schemes [31, 66] place particles throughout the domain, although Amsden [5] proposed a method that only requires particles near the surface. More recently, Chen *et al.* [16] introduced a marker particle method which uses only particles placed on the surface. The lack of connectivity information between the particles differentiates these methods from the connected front-tracking approaches by Tryggvason and collaborators [92, 91].

The particles are advected using the evolution equation,

$$\frac{d\vec{x}_p}{dt} = \vec{u}(\vec{x}_p), \tag{2.10}$$

where $\vec{x}_p$ is the position of the particle and $\vec{u}(\vec{x}_p)$ is its velocity. The particle velocities are trilinearly interpolated from the velocities on the nearest grid points. This trilinear interpolation limits the particle evolution to second order accuracy. While it is not difficult to implement higher order accurate interpolation schemes (with appropriate limiters), we have found trilinear interpolation to be sufficient and prefer it for its efficiency. We use the grid velocity at time n, although the velocity at time $n+1$ could be used as well. A third order accurate TVD Runge-Kutta method (equation 2.6) is used to evolve the particle positions forward in time.

The particles are used to both track characteristic information and to reconstruct the interface in regions where the level set method fails to accurately preserve mass. For the purpose of interface reconstruction, we allow the particles to overlap as illustrated in the bottom of figure 2.1. This allows us to reconstruct the interface exactly as the number of particles approaches infinity. Non-overlapping spheres will not accomplish this. For example, the top of figure 2.1 shows how three equally sized

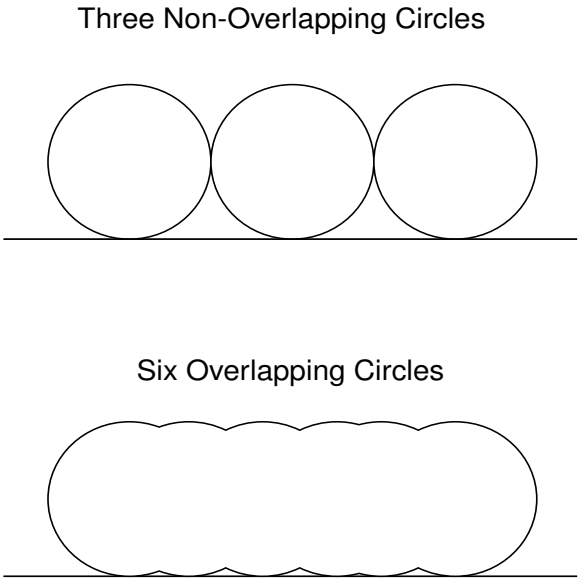

Figure 2.1: The top picture shows how three equally sized non-overlapping circles leave large spaces when attempting to represent a straight line interface, while the bottom picture shows how six equally sized overlapping circles more readily resolve the line.

non-overlapping circles leave large spaces when used to represent a straight interface, while the bottom of the figure shows that six equally sized overlapping circles more readily resolve the line. Since the particles are not physical, allowing them to overlap does not create any inconsistency in the method. The particles are used to track characteristic information, and allowing overlap merely means that some of the characteristic information is duplicated. Since the particles are allowed to overlap at the end of the time step as well, carrying around duplicate characteristic information does not hinder the scheme in any way.

For the purpose of interface reconstruction, a sphere of radius r_p is centered at each particle location, $\vec{x}_p$. The radius of each particle is bounded by minimum and maximum values based upon the grid spacing. Maximum and minimum radii which appear to work well are

$$r_{min} = .1 \min(\Delta x, \Delta y, \Delta z) \tag{2.11}$$

$$r_{max} = .5 \min(\Delta x, \Delta y, \Delta z). \tag{2.12}$$

This allows multiscale sampling of the interface by the particles. This particular choice of bounds on the particle radii (from 10% to 50% of a grid cell) was the first one we tried; further experimentation might give improved results. However, as shown in the examples section, these bounds give surprisingly good results. The reconstruction of the interface utilizing both particle and level set information is given in section 2.3.3.

We use an array based implementation to store the particle information, since connectivity information is not required. This simplifies the integration of the particle evolution equation 2.10. Certain performance optimizations of the particle array storage can be made, depending on the frequency of particle insertions and deletions. For example, one can use an oversized particle array which supports additional insertions without resizing as well as a list of the indices of valid particles so that constant repacking of the array can be avoided.

2.3 Particle Level Set Method

2.3.1 Initialization of Particles

Initially particles of both sign are randomly placed in cells that have at least one corner within $3\max(\Delta x, \Delta y, \Delta z)$ of the interface, i.e. for a given cell, we check whether $|\phi| < 3\max(\Delta x, \Delta y, \Delta z)$ at any of the eight corners. The number of particles of each type (positive or negative) per cell is set to a default of 64 particles (16 in 2D, or 4 in 1D, i.e. 4 particles per spatial dimension), although this number is user definable. An example of this initial particle seeding is shown in figure 3.1.

After the initial seeding, the particles are attracted to the correct side of the interface (i.e. positive particles to the $\phi > 0$ side and negative particles to the $\phi \leq 0$ side) into a band between a distance of $b_{min} = r_{min}$ (the minimum particle radius) and $b_{max} = 3\ \max(\Delta x, \Delta y, \Delta z)$ of the interface. The thickness of the particle bands on each side of the interface, $3\ \max(\Delta x, \Delta y, \Delta z)$ was the first we tried. One may use thinner particle bands in order to obtain better computational performance, with the caveat that this method will revert to a level set only method in regions which do not possess an adequate particle resolution of the interface. The original seeding of the

particles generates a random distribution of particles in the direction tangent to the interface. In order to obtain a random distribution of the particles in the direction normal to the interface, we chose an isocontour $\phi_{goal} \in (\pm b_{min}, \pm b_{max})$ using a uniform random distribution. Then we carry out an attraction step with the aim of placing the particle on the $\phi = \phi_{goal}$ level set contour.

The particles are attracted to the appropriate isocontours taking advantage of geometrical information contained within the level set function ϕ. Near the interface, the normal vectors give the direction to the nearest point on the interface. To attract a particle at $\vec{x}_p$ with a current interpolated level set value of $\phi(\vec{x}_p)$ to the $\phi = \phi_{goal}$ level set contour along the shortest possible path, one calculates

$$\vec{x}_{new} = \vec{x}_p + \lambda(\phi_{goal} - \phi(\vec{x}_p))\vec{N}(\vec{x}_p), \tag{2.13}$$

with $\lambda = 1$. For under-resolved regions or regions where the quality of the geometric information contained within the level set function has been degraded, equation 2.13 may not put the particle on the desired contour or even in the appropriate band. To overcome these difficulties, several iterations of this scheme may be needed. If equation 2.13 places a particle outside the computational domain, λ is halved. Then, if equation 2.13 (with this new λ) puts the particle in the appropriate band, i.e. $(\pm b_{min}, \pm b_{max})$, we accept the new particle position even though it may not be on the $\phi = \phi_{goal}$ contour. Otherwise, we halve λ once more, determine the new particle position and repeat the process with λ again initially set to 1 and $\vec{x}_p$ set to this newly calculated position. If, after a preset maximum number of iterations (e.g. we use 15), the particle is still not within the desired band, it is deleted. Figure 3.2 shows Zalesak's disk after the particle attraction step has been completed. While there are a number of particle placement strategies that could be used to accurately sample the cell including just placing the particles on their respective sides of the interface, e.g. see [27] for a discussion of "jitter", the technique discussed above worked surprisingly well as can be seen in the examples section. However, the use of more sophisticated techniques might improve the numerical results.

Finally, each particle radius is set according to

$$r_p = \begin{cases} r_{max} & \text{if } s_p\phi(\vec{x}_p) > r_{max} \\ s_p\phi(\vec{x}_p) & \text{if } r_{min} \leq s_p\phi(\vec{x}_p) \leq r_{max} \\ r_{min} & \text{if } s_p\phi(\vec{x}_p) < r_{min}, \end{cases} \tag{2.14}$$

where s_p is the sign of the particle (+1 for positive particles and -1 for negative particles). This equation adjusts the particle size such that the boundary of the particle is tangent to the interface whenever possible, while adhering to the restriction that the particle radius is bounded by r_{min} and r_{max}.

2.3.2 Time Integration

The marker particles and the level set function are separately integrated forward in time utilizing the third order accurate TVD Runge-Kutta method previously discussed. Separate temporal integration allows for the possibility of using a different ordinary differential equation solver for the particle evolution, even though we have not done so here.

2.3.3 Error Correction of the Level Set Function

The error correction of the level set function by the two sets of particles is comprised of several steps: the identification by the particles of where errors in the interface representation by the level set are occurring; calculation by each particle of the amount of error present; the combining of all of the individual particle contributions to form a reduced error representation of ϕ. Each of these steps will be discussed in more detail below. Also, we note that we apply the error correction step after each modification of the level set as shown in figure 4.3.

Identification of Error: After each complete Runge-Kutta cycle, the particles are used to locate possible errors in the level set function due to the non-physical deletion of (incorrectly perceived) merging characteristics. Particles that are on the wrong side of the interface by more than their radius, as determined by the local interpolated

$\phi(\vec{x}_p)$, are considered to have escaped. Escaped particles indicate that characteristics have probably been incorrectly merged through regularization i.e. the level set method has computed a weak solution. While not done for the examples shown in chapter 3, since these weak solutions are locally only first order accurate one could experiment with using a relatively low order accurate method for both the particle evolution and the particle correction algorithms (less accurate than the fifth order accurate WENO method used for the evolution of the level set function), due to the information provided by the lagrangian particles. This information may improves the quality of the computed results, since the particles provide characteristic information that was discarded by the level set function. Moreover, lower order accurate methods are more efficient to implement, decreasing the computational overhead.

In smooth, well resolved, regions of the flow where the level set method is highly accurate, the particles do not drift far across the interface, allowing us to retain the high order accurate level set solution. A particle is not defined as escaped when some portion of it crosses the interface. Otherwise, escaped particles would appear all the time due to numerical errors (including roundoff error). If we allowed small errors to force particle reconstruction of the level set function, we would need high order accuracy for the particle evolution and correction methods. Instead, we define a particle as escaped only when all of it crosses the interface. Since the particle radius is $O(\Delta x)$, error identification occurs only when the particle solution and the level set solution differ to first order accuracy. With at least second order accurate evolution methods for the particles and the level set function, one would not expect error identification in well resolved regions of the flow. However, in under-resolved regions where the level set method generates a first order accurate weak solution, second order accurate particle evolution will identify errors in the level set representation of the interface that need to be repaired. While one can change the escape condition for the particles, we have found that the current choice produces good numerical results.

Quantification of Error: The spheres associated with each particle can be thought of as locally defined level set functions. We represent the sphere centered at each

particle using a level set function

$$\phi_p(\vec{x}) = s_p(r_p - |\vec{x} - \vec{x}_p|) \tag{2.15}$$

where s_p is the sign of the particle, i.e ± 1. The zero level set of ϕ_p corresponds to the boundary of the particle sphere. The particle defined level set function is computed locally on the eight corners of the cell containing the particle. The local values of ϕ_p are the particle predictions of the values of the overall level set function, ϕ, on the corners of the cell. Any variation of ϕ from ϕ_p indicates possible errors in the level set solution.

Reduction of Error: We use the escaped positive particles to rebuild the $\phi > 0$ region and the escaped negative particles to rebuild the $\phi \leq 0$ region. For example, consider the $\phi > 0$ region and an escaped positive particle. The values of ϕ_p at the eight corners of the cell containing the particle are calculated using equation 2.15. Each ϕ_p is compared to the local value of ϕ and the maximum of the two values is taken as ϕ^+. This is done for all escaped positive particles creating a reduced error representation of the $\phi > 0$ region. That is, given a level set ϕ and a set of escaped positive particles E^+, we initialize ϕ^+ with ϕ and then calculate

$$\phi^+ = \max_{\forall p \in E^+} (\phi_p, \phi^+). \tag{2.16}$$

Similarly, to calculate a reduced error representation of the $\phi \leq 0$ region, we initialize ϕ^- with ϕ and then calculate

$$\phi^- = \min_{\forall p \in E^-} (\phi_p, \phi^-). \tag{2.17}$$

ϕ^+ and ϕ^- will not agree due to the errors in both the particle and level set methods as well as interpolation errors, etc. We merge ϕ^+ and ϕ^- back into a single level set

by setting ϕ equal to ϕ^+ or ϕ^-, whichever is less in magnitude at each grid point,

$$\phi = \begin{cases} \phi^+ & \text{if } |\phi^+| \leq |\phi^-| \\ \phi^- & \text{if } |\phi^+| > |\phi^-|. \end{cases} \tag{2.18}$$

The minimum magnitude is used to reconstruct the interface (instead of, for example, taking an average), since it gives priority to values that are closer to the interface.

Note that if the particle locations (from the particle evolution equation) are calculated to second order accuracy and the $O(\Delta x)$ escape condition is used, the error reduction step is needed only in regions where the level set method has computed a weak solution and deleted characteristics. Therefore, the accuracy requirements of the error reduction step can be rather low while producing markedly improved numerical results as the examples will show. While higher order accurate error reduction methods might produce better results, there is a trade off against efficiency, especially when the number of particles is large.

2.3.4 Reinitialization

Since the particle level set method relies on ϕ being an approximate signed distance function, we reinitialize the level set function using equation 2.7 after each combined Runge-Kutta cycle and error correction step. Unfortunately, reinitialization may cause the zero level set to move, which is not desirable, so we use the particle level set method to correct these errors as well.

During the reinitialization step information flows away from the $\phi = 0$ isocontour. This can be clearly seen by rewriting equation 2.7 as

$$\phi_\tau + \vec{v} \cdot \nabla\phi = \text{sgn}(\phi_0), \tag{2.19}$$

where

$$\vec{v} = \text{sgn}(\phi_0)\frac{\nabla\phi}{|\nabla\phi|}.$$

Since the normal to the interface is given by $\nabla\phi/|\nabla\phi|$, we see that equation 2.19 is a nonlinear hyperbolic equation with characteristics determined by $\vec{v}$, which point

outwards from the interface. During the reinitialization step, we *do not* want the particles to follow the characteristics associated with equation 2.19, rather we keep the particles stationary. We then use the particles to identify and correct any errors produced by the reinitialization scheme.

After reinitialization of the level set function, including the identification and reduction of errors using particles, we adjust the radii of the particles according to the current value of $\phi(\vec{x}_p)$ according to equation 2.14. This radius adjustment feeds information from the level set back to the particles, in an effort to ensure that a consistent representation of the interface by the particles and the level set function is maintained. In under-resolved regions, particles may jump (possibly relatively far) across the interface in a single time step as the level set method computes a weak solution, thereby deleting a large region of characteristic information. Through the error correction steps outline above, these first order errors can be detected and corrected for. By not deleting particle which remain escaped after each time step or allowing their radii to become zero during the radii adjustment step, information concerning any regions of deleted characteristic information is still maintained and can be incorporated by the level set function on succeeding time steps.

In summary, the order of operations is: evolve both the particles and the level set function forward in time, correct errors in the level set function using particles, apply reinitialization, again correct errors in the level set function using particles, and finally adjust the particle radii as illustrated in figure 2.2.

2.3.5 Particle Reseeding

In flows with interface stretching and tearing, regions which lack a sufficient number of particles will form. This problem has also been observed in particle-only methods which seed particles everywhere in the computational domain [30]. In order to accurately resolve the interface for all time, we need to periodically readapt the particle distribution to the deformed interface. The idea of adding and deleting particles has been proposed by many authors, see for example [46]. We not only add and delete particles in cells near the interface, but also delete particles that have drifted too

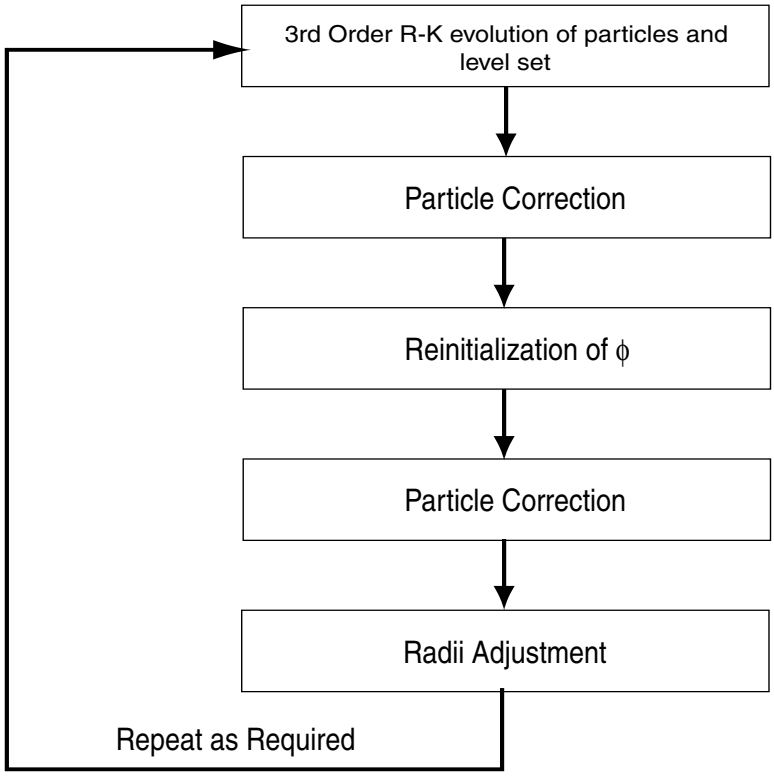

Figure 2.2: Particle Level Set computational cycle.

far from the interface to provide any useful information, e.g. positive particles with $\phi(\vec{x}_p) > b_{max}$ and negative particles with $\phi(\vec{x}_p) < -b_{max}$. The reseeding algorithm should not alter the position of the particles near the interface as they are accurately tracking the evolution of the interface and can provide useful information should they escape in the future. In addition, escaped particles should not be deleted as they indicate that characteristic information too small to be represented on the current grid has been deleted by the level set method. Even if escaped particles are not currently contributing to the level set function because there are not enough of them in a given region, they may agglomerate and contribute in the future. Moreover, recent work [11] has shown that under-resolved information can be adapted into a two phase mixture model until it reaches a critical mass where it can be reabsorbed and properly represented by the interface tracking scheme.

Reseeding is carried out by first identifying all the non-escaped particles in each

cell. Then the local value of the level set function is used to decide if a given cell is near the interface, e.g. within three grid cells. If a cell is not near the interface, all the non-escaped particles are deleted. On the other hand, if a cell near the interface has fewer particles than the previously defined maximum number (e.g. 64 in 3D), particles are added to the cell and attracted to the interface.

If there are too many non-escaped particles in a given cell, we create a heap data structure which holds the desired number of particles. Each non-escaped particle in the cell is inserted into the heap based upon the difference between the locally interpolated $\phi(\vec{x}_p)$ value and its radius, i.e. $s_p\phi(\vec{x}_p) - r_p$, since we want to keep the particles that are closest to the interface. The heap is a computationally and memory efficient way to store a priority queue. The particle with the largest $s_p\phi(\vec{x}_p) - r_p$ is placed on top. Once the heap is full and properly sorted, we consider the remaining particles one at a time. For each remaining particle, its $s_p\phi(\vec{x}_p) - r_p$ value is compared with the corresponding value of the particle atop the heap. If the current particle under consideration has a smaller value than the particle atop the heap, we delete the particle on top of the heap and replace it with the current particle. A down-heap sort is then performed placing the next candidate for removal atop the heap. If the current particle's $s_p\phi(\vec{x}_p) - r_p$ value is larger than that of the particle atop the heap, we simply delete it.

The reseeding operation is problem dependent. Viable reseeding strategies include reseeding at fixed time intervals, based upon a measure of the local curvature of the interface or according to some measure of interface stretching/compression, e.g. arc length in 2D or surface area in 3D. When reseeding based upon a change in surface area, level set methods allow easy estimation of this quantity. The surface area of the interface is given by

$$\int \delta(\phi)|\nabla\phi|d\vec{x},$$

where $\delta(\phi)$ is a numerically smeared out delta function which to first order accuracy

can be approximated as

$$\delta(\phi) = \begin{cases} 0 & \phi < -\epsilon \\ \frac{1}{2\epsilon} + \frac{1}{2\epsilon}\cos(\frac{\pi\phi}{\epsilon}) & -\epsilon \leq \phi \leq \epsilon \\ 0 & \epsilon < \phi, \end{cases}$$

where $\epsilon = 1.5\Delta x$ is the bandwidth of the numerical smearing.

Excessive reseeding is not recommended since the inserted particles have to be attracted to the interface using the current geometry defined by the level set function. If the interface geometry is poorly resolved, reseeding may not improve the resolution at the interface. In fact, it may be damaged.

In order to demonstrate the need and feasibility of the reseeding algorithm, we consider the converse to the problem addressed in figures 1.1 and 1.2. Here we use the velocity field $\vec{u} = -\vec{N}$ as opposed to the $\vec{u} = +\vec{N}$ velocity field used earlier. This velocity field is shown in figure 2.3 along with the level set initial data. In this example, the level set function experiences a rarefaction at the corners as a single point expands into the quarter circle as shown in figure 2.4. Figure 2.5 shows an initial seeding of passively advected interior particles while figure 2.6 shows the final location of these particles. Note that they have spread out appreciably in the corners. Figure 2.7 shows the same result after one application of the reseeding algorithm. The interface is now significantly more accurately resolved by the particles.

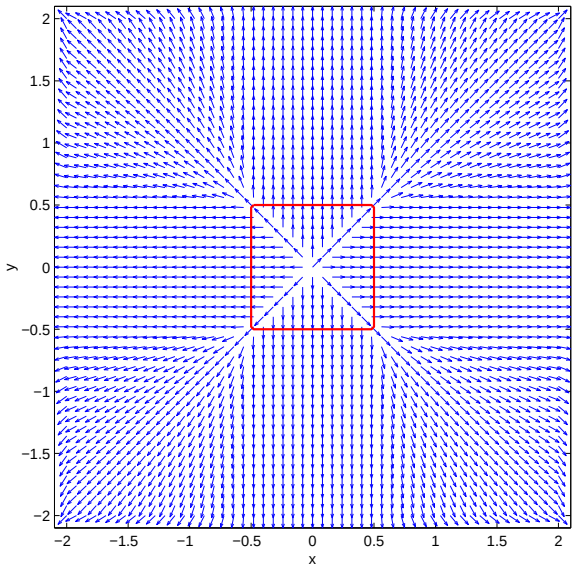

Figure 2.3: Expanding square. Initial interface location and velocity field.

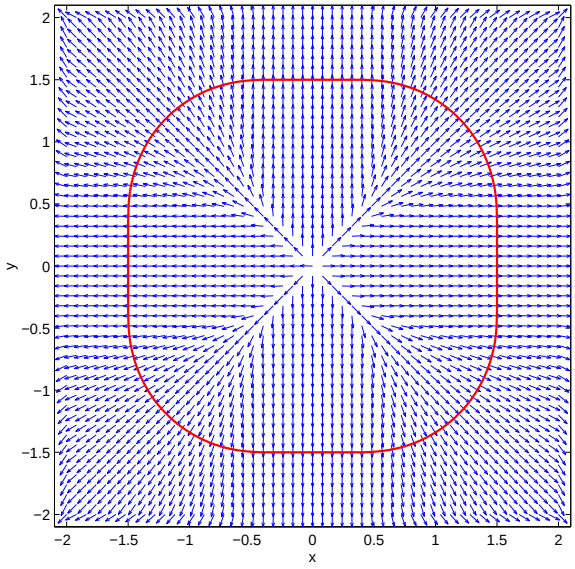

Figure 2.4: Expanding square. Final interface location of the level set solution.

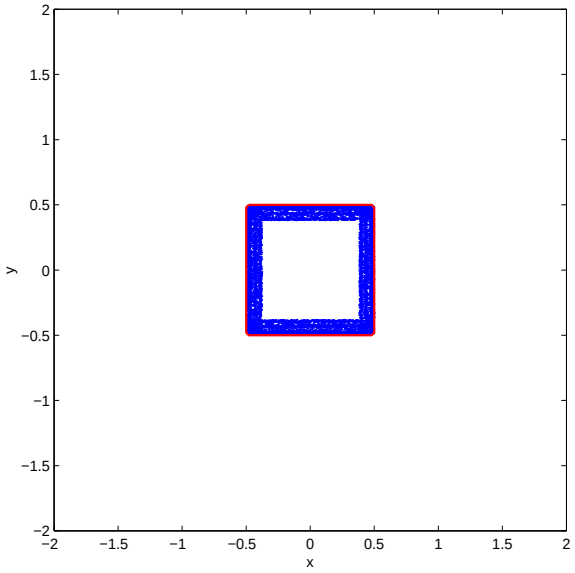

Figure 2.5: Expanding square. Passively advected particles are initially seeded inside the interface.

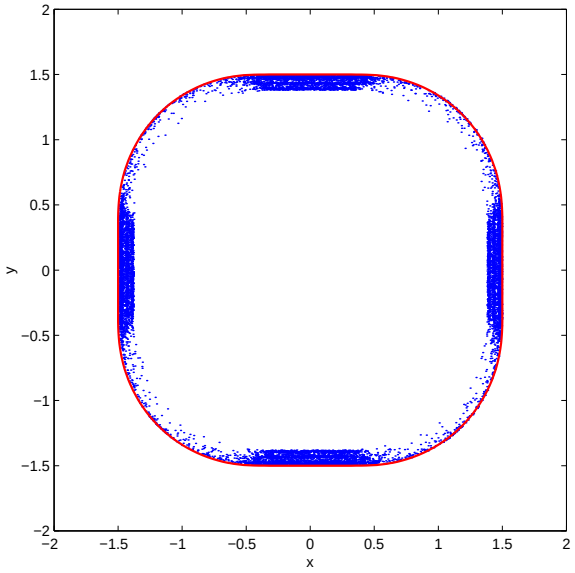

Figure 2.6: Expanding square. Final location the passively advected marker particles.

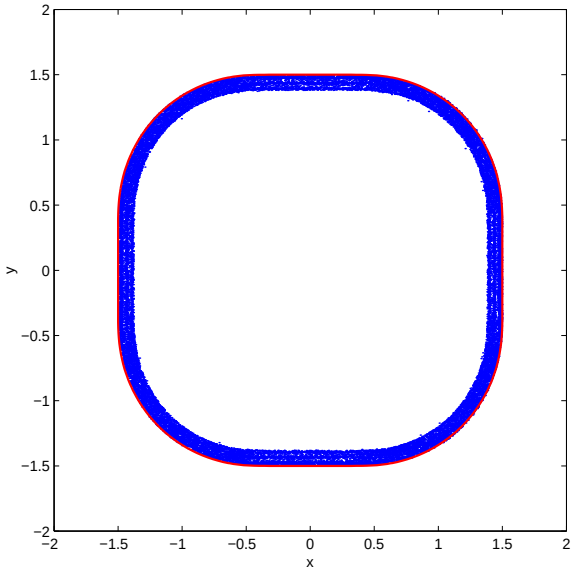

Figure 2.7: Expanding square. Location of interior particles after one application of the reseeding algorithm.

Chapter 3

Examples

3.1 Rigid Body Rotation of Zalesak's Disk

Consider the rigid body rotation of Zalesak's disk in a solid body velocity field [96]. The initial data is a slotted circle centered at (50,75) with a radius of 15, a width of 5, and a slot length of 25. The velocity field is given by

$$\begin{aligned} u &= (\pi/314)(50 - y), \\ v &= (\pi/314)(x - 50), \end{aligned}$$

so that the disk completes one revolution every 628 time units.

Figure 3.1 illustrates the initial seeding of particles on both sides of the interface while figure 3.2 depicts the particle locations after the attraction step has been applied to attract them to the appropriate bands on the correct side of the interface. Blue dots indicate the locations of negative particles and red dots indicate the locations of positive particles. A 100×100 grid cell computational mesh is shown in the figures, showing that the slot is only 5 grid cells across.

Figure 3.3 illustrates the high quality particle level set solution obtained after one full rotation. Figures 3.4 and 3.5 compare the evolution of a level set only method (red) and our particle level set method (blue) after one and two revolutions, respectively. The exact solution (green) is also plotted for the sake of comparison.

As expected, the level set only method applies an excessive amount of regularization in the sharp corners.

Figure 3.6 illustrates the need for both positive and negative particles. Here, we plot the level set solution, the particle level set solution and the exact solution along with both the positive and negative particles. The errors in the level set solution are emphasized by plotting escaped positive particles in light red and the escaped negative particles in light blue. This illustrates how the positive particles correct the errors at the two corners at the top of the slot while the negative particles correct the errors at the two corners near the bottom of the slot.

Tables 3.1 and 3.2 compare the area loss (or gain) of the level set method and the particle level set method on three different grids. The area is calculated using a second order accurate unbiased level set contouring algorithm [10]. In addition, we calculate the accuracy of the interface location using the first order accurate error measure introduced in [83],

$$\frac{1}{L}\int |H(\phi_{expected}) - H(\phi_{computed})|dxdy, \tag{3.1}$$

where L is the length of the expected interface. This integral is numerically calculated as in [83]:

- partition the domain into many tiny pieces (1000×1000),
- interpolate $\phi_{computed}$ onto the newly partitioned domain and calculate $\phi_{expected}$ for the domain,
- numerically integrate equation 3.1, where $H(\phi)$ is the indicator function for $\phi \leq 0$, i.e. $H(\phi) = 1$ if $\phi \leq 0$ and $H(\phi) = 0$ otherwise.

On the coarsest grid (50×50 grid cells), the level set only solution vanishes before one revolution is completed while the particle level set method still maintains 83.8% of the area even after two rotations.

	Grid Cells	Area	% Area Loss	L_1 Error	Order
	exact	582.2	-	-	-
One Revolution	50	0	100%	4.03	N/A
	100	613.0	-5.3%	.61	2.7
	200	579.1	.54%	.08	2.9
Two Revolutions	50	0	100%	4.03	N/A
	100	634.7	-9.0%	.89	2.2
	200	577.4	.82%	.11	3.0

Table 3.1: Zalesak's disk. Level set method.

	Grid Cells	Area	% Area Loss	L_1 Error	Order
	exact	582.2	-	-	-
One Revolution	50	495.7	14.9%	.59	N/A
	100	580.4	.31%	.07	3.1
	200	581.0	.20%	.02	1.5
Two Revolutions	50	487.6	16.2%	.62	N/A
	100	578.0	.72%	.09	2.8
	200	580.0	.38%	.03	1.4

Table 3.2: Zalesak's disk. Particle level set method.

3.2 Single Vortex

While the Zalesak's disk problem is a good indicator of diffusion errors in an interface capturing method, it does not test the ability of an Eulerian scheme to accurately resolve thin filaments which can occur in stretching and tearing flows. A flow which exhibits interface stretching is the "vortex-in-a-box" problem introduced by Bell, Colella and Glaz [8]. Figure 3.7 shows the non-constant vorticity velocity field centered in the box with the largest velocity located half way to the walls of the domain. The velocity field is defined by the stream function

$$\Psi = \frac{1}{\pi}\sin^2(\pi x)\sin^2(\pi y).$$

A unit computational domain is used with a circle of radius .15 placed at (.5,.75). The velocity field stretches the circle into a very long, thin fluid element which progressively wraps itself towards the center of the box.

Figure 3.8 shows the location of the particles at $t = 1$ using a 64×64 grid. The positive particles are shown in red while the negative particles are shown in blue. Even at this relatively early time, there has been a substantial stretching of the interface, and the particle bands which were initially three grid cells deep have been stretched and compressed. Both the particle level set solution and a high resolution front tracked solution are plotted in the figure, although it is difficult to ascertain which is which as they are almost on top of each other. The role of the particles in helping to maintain the interface can be seen in figure 3.9 which depicts the level set solution along with light blue negative particles that have escaped from the level set solution. Note that escaped particles are found at both the head and tail where the curvature is large.

The ability of the particle level set method to maintain thin, elongated filaments is shown in figures 3.10 (at $t = 3$) and 3.11 (at $t = 5$). These figures were computed using 128×128 grid cells. The interface is depicted in figure 3.10 is at the same time as in figure 13a in [68] and figures 4a,b,c,d in [67] for the sake of comparison. Both figures show the level set solution (red), the particle level set solution (blue) and the high resolution front tracked solution (green). The particle level set method clearly outperforms the level set method. Only near the head and the tail of the interface where the level set is about one grid cell wide does the particle level set method fail to compete with the high resolution front tracked solution. Also note that while the particle level set method does not conserve area it exhibits less "blobby" structure than VOF methods, see figure 4d in [67]. In under-resolved regions, the particles are not close enough together to accurately represent the interface and thin filaments will break apart. However, the particles still track the interface motion with second order accuracy so the resulting pieces are in accurate locations. In contrast, the interface reconstruction procedure used in VOF methods forces mass in neighboring cells to artificially clump together. As a result, mass in under-resolved regions is moved inaccurately during the interface reconstruction step, resulting in larger blobs with first order accurate errors in their location.

For purposes of error analysis, the velocity field is time reversed by allowing the velocity to have $\cos(\pi t/T)$ time dependence where T is the time at which the flow

Grid Cells	Area	% Area Loss	L_1 Error	Order
exact	.0707	-	-	-
64	0	100.0%	.075	N/A
128	.0425	39.8%	.031	1.3
256	.0634	10.3%	.008	2.0

Table 3.3: One period of vortex flow. Level set method.

Grid Cells	Area	% Area Loss	L_1 Error	Order
exact	.0707	-	-	-
64	.0694	1.81%	.003	N/A
128	.0702	.71%	.001	1.1
256	.0704	.35%	5.09E-4	1.4

Table 3.4: One period of vortex flow. Particle level set method.

returns to its initial state, see LeVeque [47]. The reversal period used in the error analysis of the vortex problem is $T = 8$ producing a maximal stretching of the interface similar to that shown in figure 3.10. As can be seen from the error tables 3.3 and 3.4 as well as figures 3.12 and 3.13, the ability of the particle level set method to model interfaces undergoing substantial stretching is quite good. The L_1 errors reported here compare favorably with those reported by Rider and Kothe in [68] using a VOF PLIC method.

3.3 Deformation Field

An even more difficult test case is the entrainment of a circular body in a deformation field defined by 16 vortices as introduced by Smolarkiewicz [77]. The periodic velocity field is given by the stream function

$$\Psi = \frac{1}{4\pi} \sin(4\pi(x + .5)) \cos(4\pi(y + .5)). \tag{3.2}$$

Periodicity is enforced so the portion of the interface that crosses the top boundary of the domain reappears on the bottom as shown in figure 3.14 at $t = 1$. The velocity field given by equation 3.2 is made periodic in time by multiplying the velocity

Grid Points	Area	% Area Loss	L_1 Error	Order
exact	.0707	-	-	-
64	.0569	19.5%	.045	N/A
128	.0585	17.2%	.016	1.5
256	.0622	12.0%	.009	.8

Table 3.5: One period of deformation flow. Level set method.

Grid Points	Area	% Area Loss	L_1 Error	Order
exact	.0707	-	-	-
64	.0696	1.59%	.002	N/A
128	.0705	.03%	.001	1.1
256	.0705	.03%	4.4E-4	1.4

Table 3.6: One period of deformation flow. Particle level set method.

components by $\cos(\pi t/T)$, with $T = 2$. The figure shows the level set solution (red), the particle level set solution (blue) and the high resolution front tracked solution (green) using a 128×128 grid. Note that the widths of some of the filamentary regions are of the order of a grid cell and would be very difficult to resolve without the information provided by the particles. One can increase the particle resolution of the interface by several techniques. More particles can be added at the beginning of the simulation by increasing the particles' initial bandwidth or the number of particles per cell. In addition, one could periodically apply reseeding, although caution should be used when reseeding the interface shown in figure 3.14 as the geometry is poorly defined in the under-resolved regions.

As can be seen from the error tables 3.5 and 3.6 as well as figures 3.15 and 3.16, the ability of the particle level set method to model interfaces undergoing substantial stretching is quite good.

3.4 Rigid Body Rotation of Zalesak's Sphere

In analogy with the two dimensional Zalesak disk problem, we use a slotted sphere to examine the diffusion properties of the particle level set method in three spatial dimensions. The sphere has radius 15 in a $100 \times 100 \times 100$ domain. The slot is 5 grid

cells wide and 12.5 grid cells deep on a $100 \times 100 \times 100$ grid cell domain. The sphere is initially placed at $(50, 75, 50)$ and undergoes rigid body rotation in the $z = 50$ plane about the point $(50, 50, 50)$. The constant vorticity velocity field is given by

$$\begin{aligned} u(x, y, z) &= (\pi/314)(50 - y), \\ v(x, y, z) &= (\pi/314)(x - 50), \\ w(x, y, z) &= 0, \end{aligned}$$

so that the sphere completes one revolution every 628 time units.

The presence of an extra dimension allows for more opportunities to examine an interface capturing scheme for excessive amounts of regularization. Figures 3.17 and 3.18 show the level set and the particle level set solutions, respectively, at approximately equally spaced time intervals from $t = 0$ to $t = 628$. The final frame at $t = 628$ should be identical to the initial data at $t = 0$. The particle level set method is able to maintain the sharp features of the notch while the level set method is unable to do so.

In order to illustrate the volume preservation properties of our scheme, we estimate the volume of the interior region using a first order accurate approximation to the integral

$$\int H(\phi) d\vec{x} \tag{3.3}$$

where H is a numerically smeared out Heaviside function given by

$$H(\phi) = \begin{cases} 0 & \phi < -\epsilon \\ \frac{1}{2} + \frac{\phi}{2\epsilon} + \frac{1}{2\pi} \sin\left(\frac{\pi\phi}{\epsilon}\right) & -\epsilon \leq \phi \leq \epsilon \\ 1 & \epsilon < \phi \end{cases} \tag{3.4}$$

with $\epsilon = 1.5\triangle x$ the bandwidth of the numerical smearing. It is interesting to note that the level set solution loses only 2.1% of its total volume while the particle level set solution has lost 2.3%. The level set method has both inward and outward dissipation errors in convex and concave regions, respectively, leading to a fortuitous cancellation and a misleading appearance of accuracy with respect to volume preservation alone.

Similar statements hold for VOF calculations that preserve volume almost exactly, but locate the volume incorrectly, e.g. the creation of spurious flotsam and jetsam.

3.5 Three Dimensional Deformation Field

LeVeque [47] proposed a three dimensional incompressible flow field which combines a deformation in the x-y plane with one in the x-z plane. The velocity field is given by

$$\begin{aligned} u(x,y,z) &= 2\sin^2(\pi x)\sin(2\pi y)\sin(2\pi z), \\ v(x,y,z) &= -\sin(2\pi x)\sin^2(\pi y)\sin(2\pi z), \\ w(x,y,z) &= -\sin(2\pi x)\sin(2\pi y)\sin^2(\pi z) \end{aligned}$$

and the flow field is modulated in time with a period of $T = 3$. A sphere of radius .15 is placed within a unit computational domain at $(.35, .35, .35)$. A $100 \times 100 \times 100$ grid cell domain was used. This allows the sphere to be entrained by two rotating vortices which initially scoop out opposite sides of the sphere and then compress them causing the sphere to pancake. The top and bottom edges of the pancake are then caught up again in the vortices causing the surface to become very stretched. Parts of the interface thin out to about a grid cell and both methods have difficulty resolving this thin interface. Of course, we could use a variety of techniques to increase the initial particle density or to reseed along the way, but the particle level set method recovers rather nicely and loses very little volume even without increasing the particle count. On the other hand, the level set method fails severely in this example.

Figures 3.19 and 3.20 show the level set solution and the particle level set solution, respectively, at $t = 0$, $10\triangle s$, $20\triangle s$, $30\triangle s$, $40\triangle s$, $50\triangle s$, $60\triangle s$, $70\triangle s$, $90\triangle s$, $110\triangle s$, $130\triangle s$ and $150\triangle s$ where $\triangle s = 628/150$. The final frame at $t = 150\triangle s$ should be identical to the initial data at $t = 0$. In addition, frame $130\triangle s$ should be identical to frame $20\triangle s$, frame $110\triangle s$ should be identical to frame $40\triangle s$, and frame $90\triangle s$ should be identical to frame $60\triangle s$. The maximum stretching occurs at $t = 75\triangle s$ where the level set solution has lost 49% of the initial volume and the particle level set solution

has gained 1.9%. After completing a full cycle, at $t = 150\triangle s$, the level set solution has lost 80% of the initial volume while the particle level set solution has only lost 2.6%.

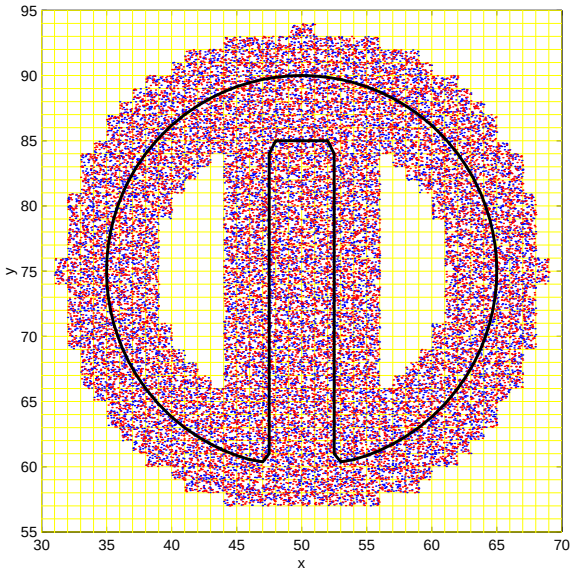

Figure 3.1: Initial placement of particles on both sides of the interface.

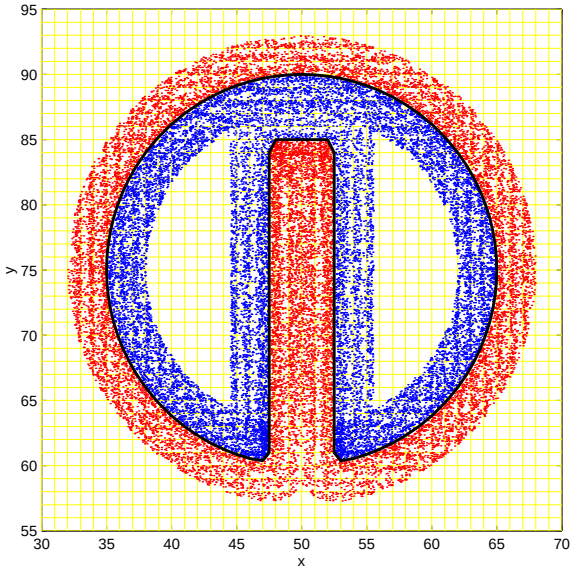

Figure 3.2: Particle positions after the initial attraction step.

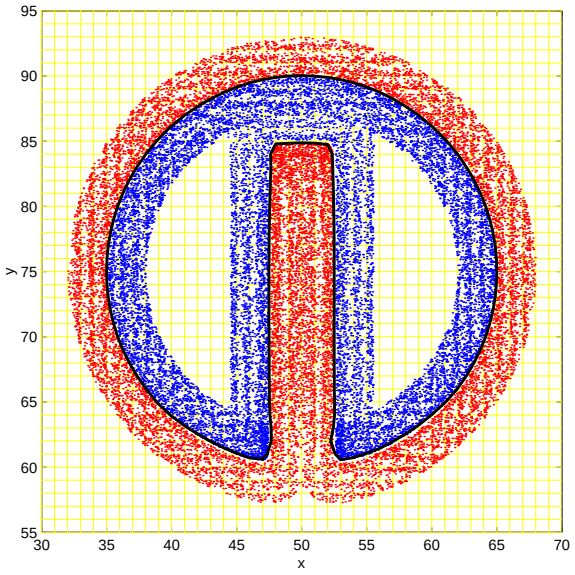

Figure 3.3: Particle level set solution after one revolution.

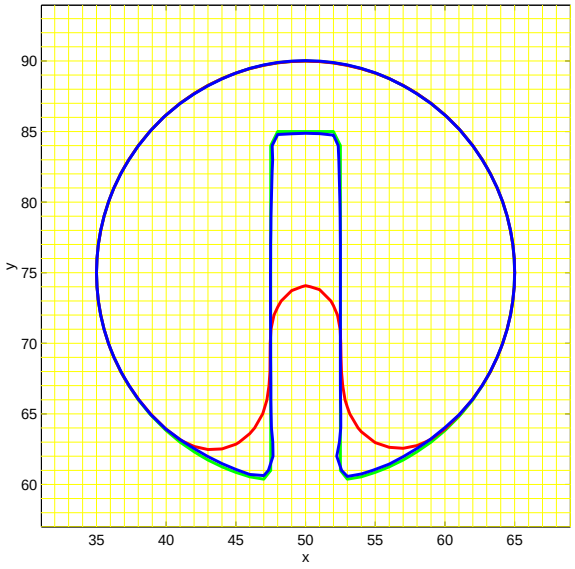

Figure 3.4: Comparison of the level set solution (red), particle level set solution (blue) and theory (green) after one revolution.

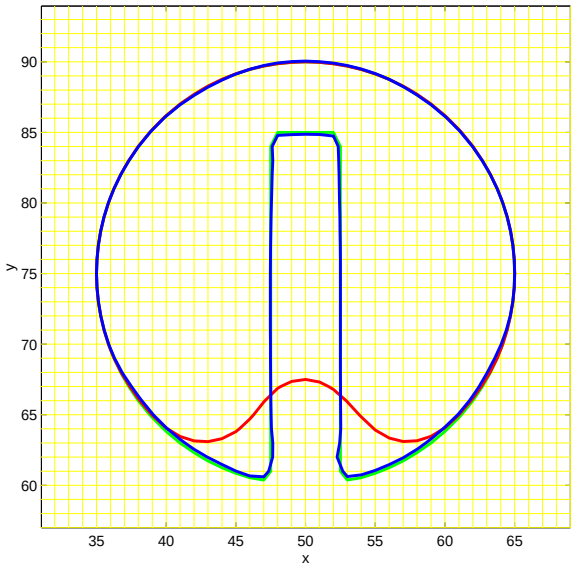

Figure 3.5: Comparison of the level set solution (red), particle level set solution (blue) and theory (green) after two revolutions.

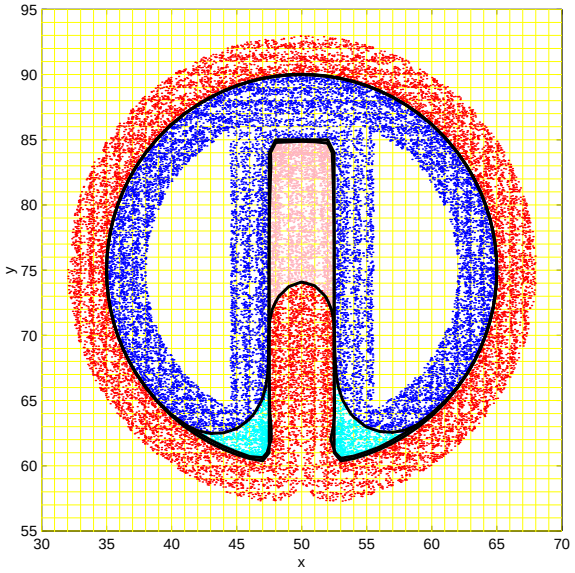

Figure 3.6: Comparison of the level set solution, particle level set solution and theory after one revolution. The light red particles and light blue particles have escaped from the level set solution.

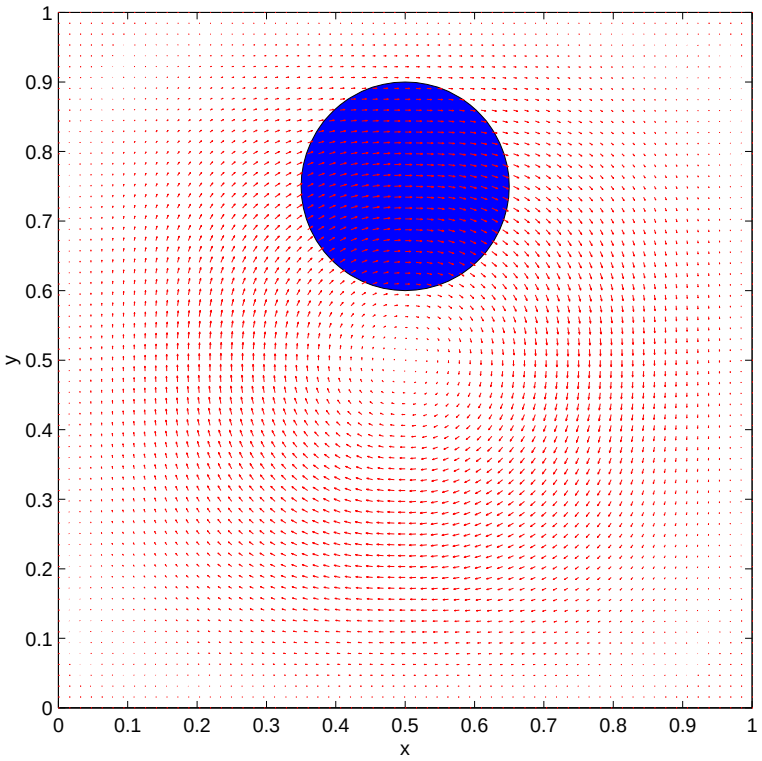

Figure 3.7: Initial data and velocity field for the vortex flow.

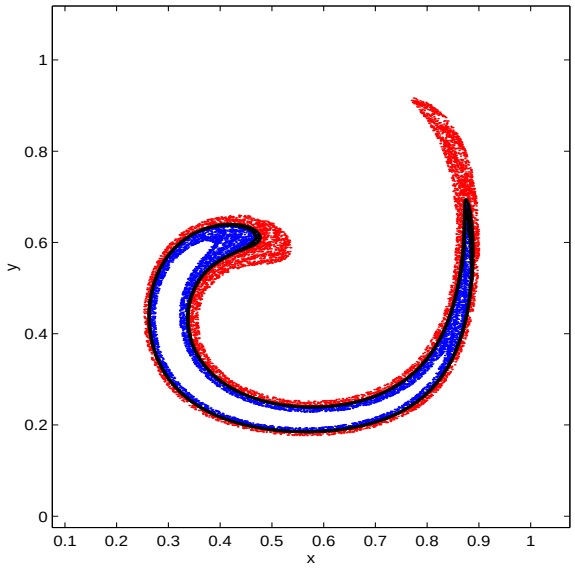

Figure 3.8: Comparison of the particle level set solution and a high resolution front tracked solution for the vortex flow at $t = 1$.

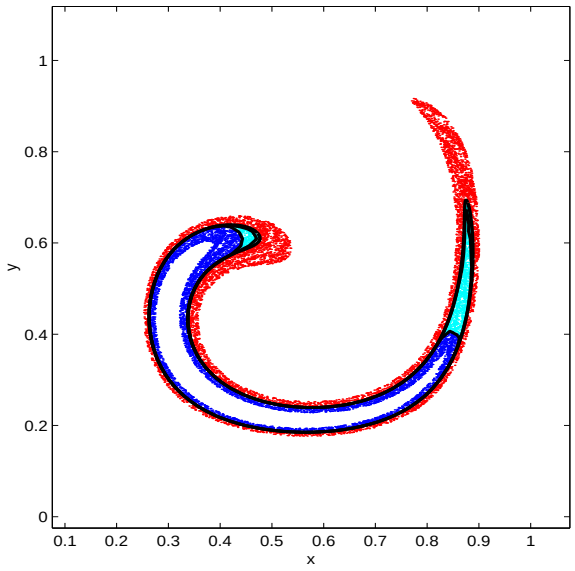

Figure 3.9: Comparison of the level set solution, particle level set solution and a high resolution front tracked solution for the vortex flow at $t = 1$. The light blue particles have escaped from the level set solution.

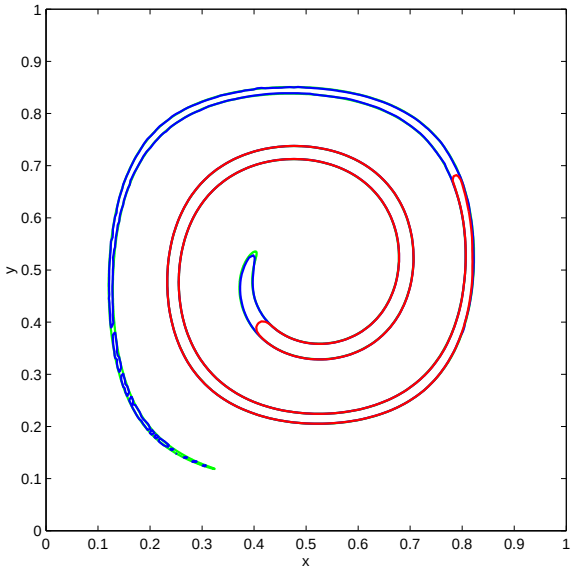

Figure 3.10: The level set solution (red), particle level set solution (blue) and a high resolution front tracked solution (green) for the vortex flow at $t = 3$.

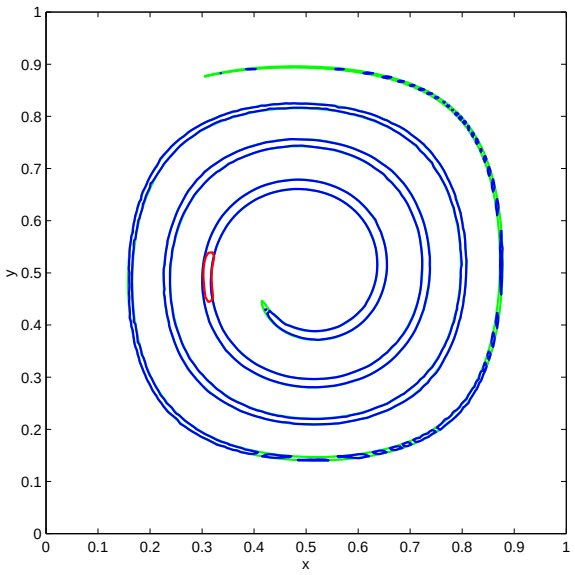

Figure 3.11: The level set solution (red), particle level set solution (blue) and a high resolution front tracked solution (green) for the vortex flow at $t = 5$.

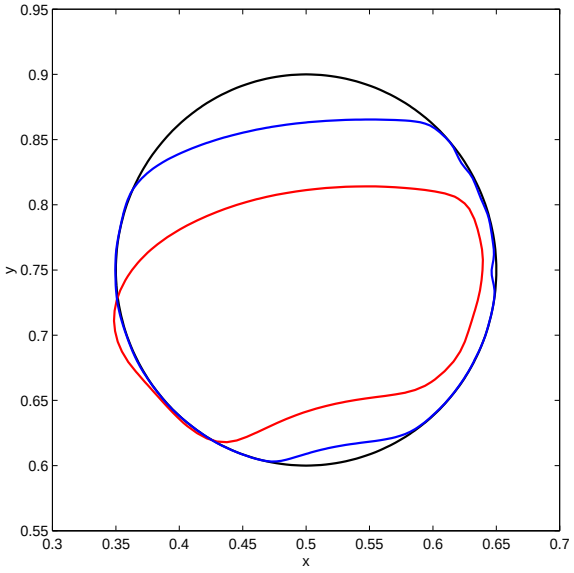

Figure 3.12: Level set solution. The exact solution (black) in comparison to grids of size 256×256 (blue), 128×128 (red) and 64×64 (green - disappeared).

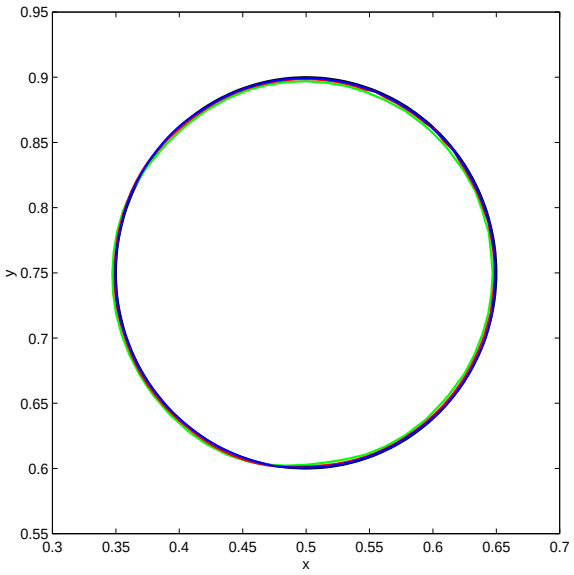

Figure 3.13: Particle level set solution. The exact solution (black) in comparison to grids of size 256×256 (blue), 128×128 (red) and 64×64 (green).

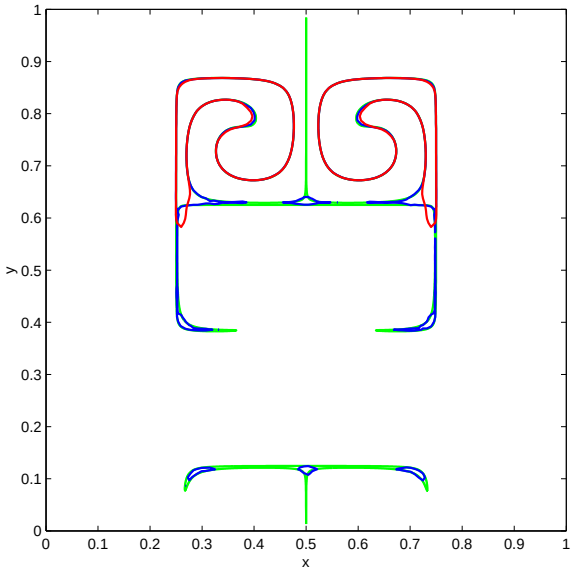

Figure 3.14: Comparison of the level set solution (red), particle level set solution (blue) and a high resolution front tracked solution (green) for the deformation flow at $t = 1$.

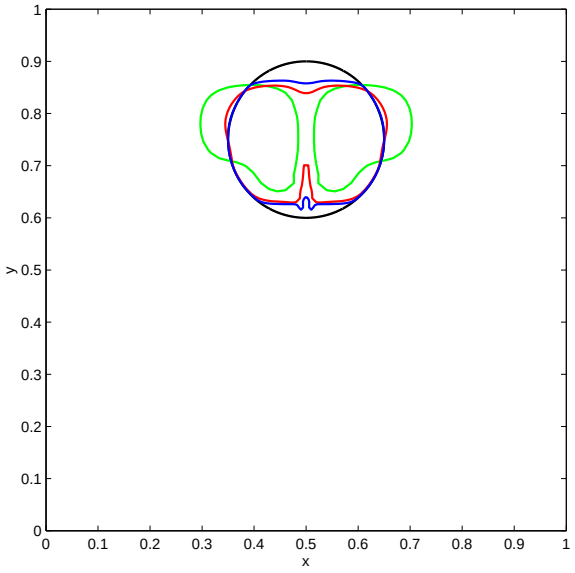

Figure 3.15: Level set solution. The exact solution (black) in comparison to grids of size 64×64 (green), 128×128 (red) and 256×256 (blue).

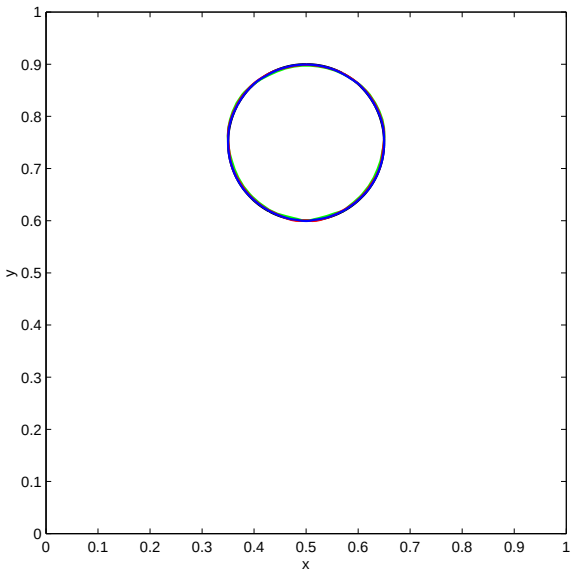

Figure 3.16: Particle level set solution. The exact solution (black) in comparison to grids of size 64×64 (green), 128×128 (red) and 256×256 (blue).

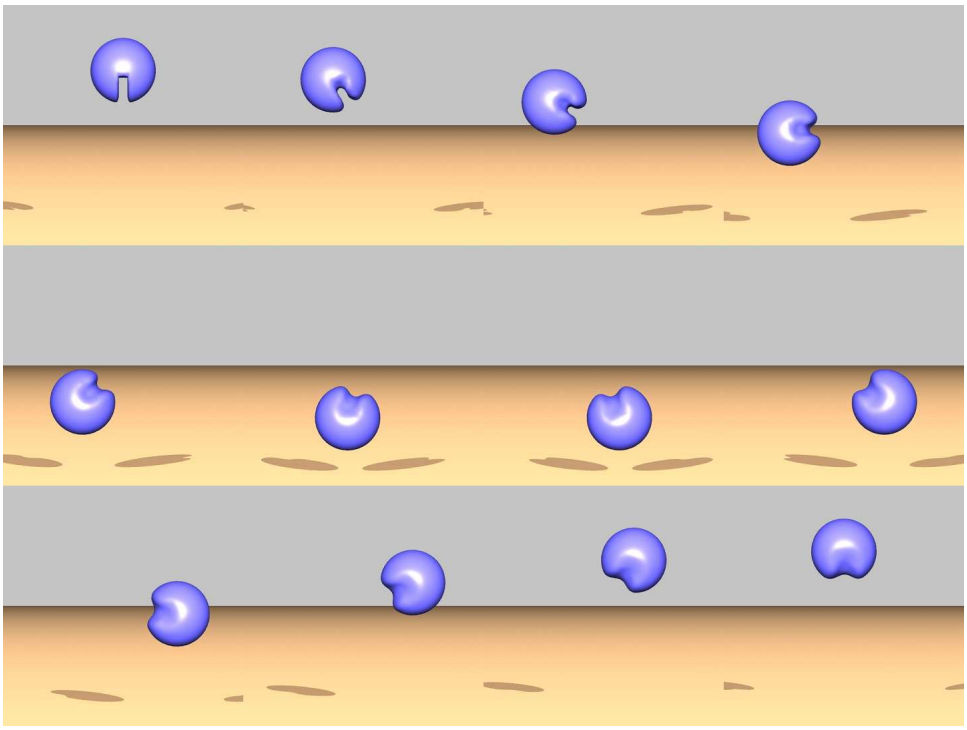

Figure 3.17: Zalesak's sphere. Level set solution.

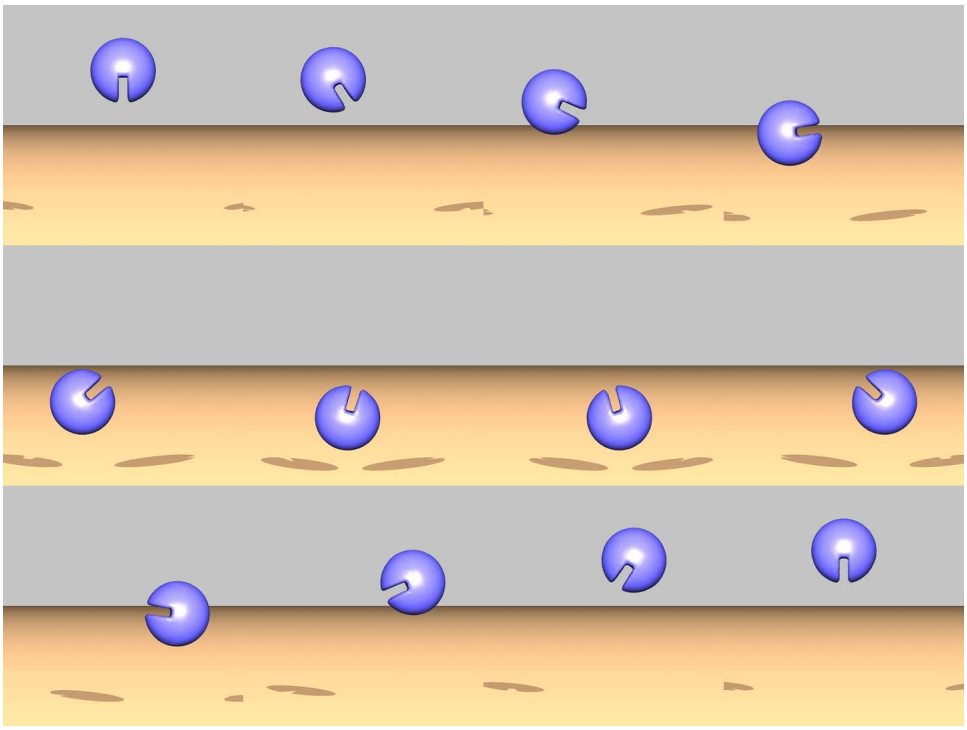

Figure 3.18: Zalesak's sphere. Particle level set solution.

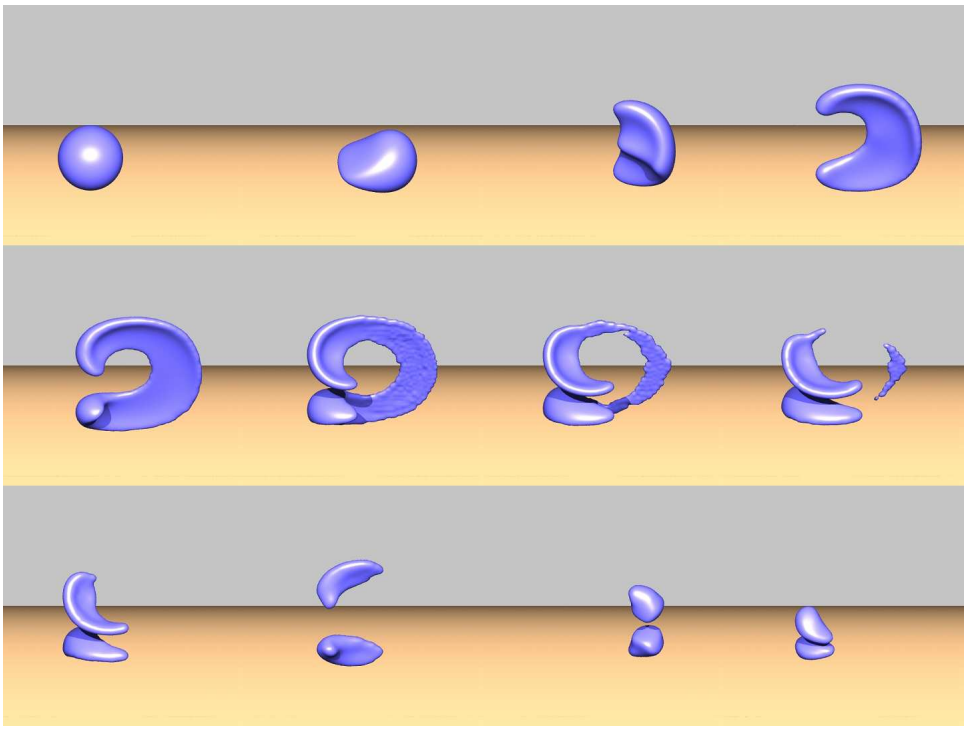

Figure 3.19: Deformation test case. Level set solution.

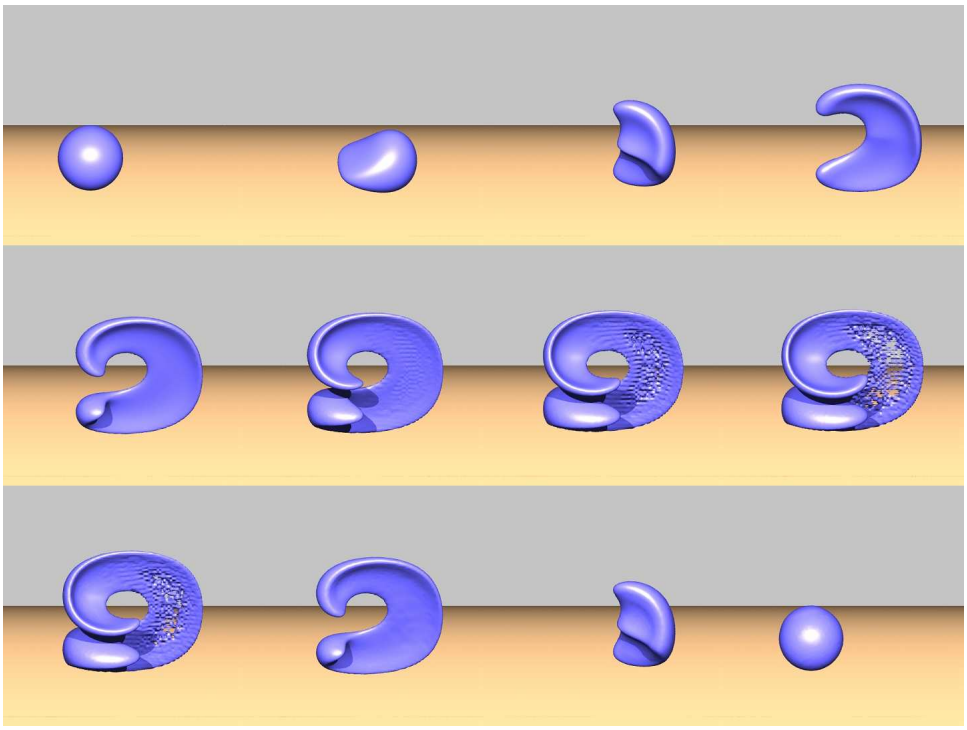

Figure 3.20: Deformation test case. Particle level set solution.

Chapter 4

Free Surface Calculations

"In the time honored tradition of computer graphics,
we can now go ahead and steal anything we can get."
Fournier and Reeves [26]

4.1 Liquid Free Surface Flows

The ubiquity of water in our everyday lives has motivated scientists and engineers to attempt to simulate a wide variety of liquid phenomena. The simulation of the destructive force of tsunamis and waves on beaches [48, 40, 29]; the breakup of thin sheets of liquid fuel [49, 43] or the formation of ink drops for printing [4]; the filling of containers for food industry applications [88, 87]; and the adhesion of two circulatory cells under shear flow [3], has prompted the development of a wide variety of novel methods to describe the motion of the liquid and the free surface present in each of these applications. A common theme among all of these applications is the complex, three-dimensional behavior of the interface. Any method used to describe the behavior of the free surface needs to be capable of capturing these aspects of water surfaces. Besides the obvious economic and environmental importance of being able to develop mechanisms to control the liquid through improved numerical modeling, the lively, complex motion of the free surface is often visually attractive to the casual observer. This attractiveness has recently motivated the computer graphics community to take

an interest in the realistic animation of complex water surfaces.

4.2 CFD and Computer Animation

The use of computational fluid dynamics to mimic liquid behavior for purposes of computer animation is a relatively recent phenomenon. While the engineering and scientific communities wish to achieve the highest fidelity possible in a simulation, the animation community does not need to achieve this goal. Rather, the goal is to achieve a "believable" liquid performance. This liberates the animator from being forced to use a realistic model of a liquid. While the animator has a lot of freedom as to how to animate a liquid, liquids are governed by certain physical laws so it makes sense that an animator will utilize simplifying assumptions in order to obtain the desired performance. This approach to the animation of liquids has been used extensively by the animation community. Original efforts to obtain two dimensional wave behavior is seen in the efforts of Masten [51] using Fourier synthesis techniques and Schachter [69] with a parametric representation of the water surface. Peachey [61] borrowed features of Airy models and Fournier and Reeves [26] utilized Gerstner wave theory to generate realistic looking periodic waves which appear to almost break.

To obtain more realistic liquid performances, the animation community then turned towards two dimensional approximations to the full three dimensional Navier-Stokes equations. A height field representation of the water surface used by Kass and Miller [42] was derived from a linearized form of the two dimensional shallow water equations. Interaction with obstacles using a pressure determined height field formulation was used by Chen and Lobo [14]. Two dimensional splashing liquids with spray being modeled by particles was presented in [57]. As an alternative to Navier-Stokes models, a viscous spring-particle representation of a liquid has been proposed by Miller and Pearce [53] and a molecular dynamics approach was used in [86].

While the above approaches have been and continue to be used in the animation community, exciting and dynamic water behavior can only result from the use of fully three dimensional computational fluid dynamics algorithms. Foster and Metaxas [25]

built upon the original CFD work of Harlow and Welch [31] in creating a 3D Navier-Stokes methodology for the realistic animation of liquids. A staggered flow grid arrangement was used along with a marker particle representation of the liquid. Both the convective and viscous terms were discretized using central differencing and the entire system was integrated in time using a forward Euler scheme. In the case of animating water or other relatively inviscid substances, the combination of spatial central differencing for the convective terms and a forward Euler time discretization can pose a severe time step restriction, i.e. $\Delta t \sim (\Delta x)^2$, for the simulation to remain stable. Even if upwind differencing is used for the convection terms, a CFL condition of $u\Delta t/\Delta x < 1$ will need to be obeyed. Stam in 1999 [78] proposed a "Stable Fluid" approach to the treatment of the convective term in the Navier-Stokes equations for animation applications. This "Stable Fluid" approach is really a semi-Lagrangian method first proposed in 1952 by Courant, Issacson, and Rees [20]. Besides its proposed use in the animation community, semi-Lagrangian methods are popular in the meteorological community for their stability characteristics [52, 79]. Use of a semi-Lagrangian method allows a liquid animation to remain stable even when using time steps larger than that given by a traditional CFL condition for Eulerian finite difference schemes, providing tremendous computational savings by reducing the number pressure calculations done at the cost of introducing additional amounts of numerical viscosity.

While the seminal work of Foster and Metaxas introduced the use of fully three dimensional Navier-Stokes simulations for the purposes of animating liquids, the practical application of CFD technology for liquid animations was introduced by Foster and Fedkiw [24]. Some of these contributions include:

- A semi-Lagrangian "Stable Fluid" approach for the convective terms in order to minimize number of expensive pressure iterations;
- Use of a novel hybrid liquid volume model combining a level set and marker particle approach to represent the liquid;
- Time step subcycling for the evolution of particles and level set in order to maintain stability of the interface given CFL violating large liquid time steps;

- Use of an efficient Preconditioned Conjugate Gradient method to solve for the pressure during the projection step, unlike the slow SOR method used by Foster and Metaxas;

- Formulation of plausible velocity boundary conditions for moving objects in the liquid.

The combination of all of these technologies has begun to meet the engineering requirements for the use of fully three dimensional computational fluid dynamics algorithms in a computer animation environment. Utilization of inherently *stable* algorithms to avoid having animators not trained in computational methods perform costly numerical stability studies; use of *fast* numerical algorithms for quick turn around time; *robust and accurate* interface methods used to convey the presence of the free surface even on the coarse grids commonly used by animators; and *interactive* algorithms which allows for the possibility of controlling the behavior of the liquid and the ability for the liquid to affect the motion of objects and vice versa.

We wish to focus for a moment on the hybrid volume model utilized by Foster and Fedkiw to model the free surface of the liquid. The use of a level set only representation for the interface introduces difficulties in maintaining the liquid volume on the coarse grids commonly used in an animation environment as discussed in Chapter 2. This difficulty was recognized by Foster and Fedkiw and marker particles were used to represent the volume of liquid in regions of high curvature near the interface. To illustrate the behavior of the hybrid volume model, the resulting interface after one rotation of Zalesak's disk is shown in figure 4.1(c). The Foster and Fedkiw scheme does an excellent job of preserving the liquid volume as compared to a level set only method, but it is at the expense of not preserving the air in the notch. The problem with the hybrid volume model is that it does not model the opposite side of the interface, the air side of the interface in this case. The particle level set result on the other hand as seen in figure 4.1(d) does not favor one side of the interface over the other and is able to maintain the sharpness of the notch.

While CFD algorithms have been slowly working their way into a traditional production animation environment [95], the combination of all of the above technologies

has made it feasible to perform fully three dimensional simulations for animating liquids.

4.3 Liquid Model

4.3.1 Navier-Stokes Equations

Our simulations utilize the three dimensional Navier-Stokes equations given by

$$\vec{u}_t = -\vec{u} \cdot \nabla \vec{u} + \nu \nabla \cdot (\nabla \vec{u}) - \frac{1}{\rho} \nabla p + \vec{g}, \tag{4.1}$$

where $\vec{u} = (u, v, w)$ is the velocity, ν is the kinematic viscosity of the liquid, ρ is the density of the liquid, p is the pressure, and $\vec{g}$ is an externally applied gravity field. While nothing in our computational scheme precludes the simulation of highly viscous flows, the viscosity of water is negligible so we do not explicitly model the second term on the right hand side of equation 4.1. In order to calculate the pressure we impose the incompressibility constraint on the liquid resulting from the law of conservation of mass,

$$\nabla \cdot \vec{u} = 0. \tag{4.2}$$

At a wall, we choose to apply a flow tangency boundary condition. If we define $\vec{N}$ to be the normal to the wall and $\vec{T}_1$ and $\vec{T}_2$ to be two mutually orthogonal tangent vectors to the wall, we impose

$$\vec{u} \cdot \vec{N} = 0 \tag{4.3}$$

$$\nabla \vec{u} \cdot \vec{T}_1 = \nabla \vec{u} \cdot \vec{T}_2 = 0. \tag{4.4}$$

By performing the simulation using a staggered velocity-pressure (MAC grid) arrangement we can avoid specifying a pressure boundary condition at the wall. The velocity and pressure boundary conditions at the free surface are discussed below.

The boundary conditions we impose in the presence of objects placed in the liquid are discussed in section 4.5.3.

Finally, we usually begin the simulation with a specified velocity field and an initial position for the free surface.

4.3.2 Free Surface Boundary Conditions

We do not solve equations 4.1 and 4.2 over the entire computational domain, but only in the regions occupied by the liquid. Our calculations do not model the dynamics of the air on the free surface as in a truly multiphase calculation. In general, two boundary conditions apply at the free surface:

- The *kinematic condition* states that there is no transport of mass through the interface. Mathematically we can represent this condition as

$$[\vec{u} - \vec{u}_{fs}]_{fs} \cdot \vec{N} = 0, \tag{4.5}$$

  where $\vec{u}_{fs}$ is the velocity of the free surface and the jump condition is taken at the boundary. Practically, this means that the level set should take as its velocity field that of the fluid and the marker particles should interpolate their velocity from the fluid velocity.

- The *dynamic condition* is a statement of momentum conservation at the free surface, i.e. the fluid forces at the free surface are in equilibrium. In general, the presence of surface tension causes a jump in the normal stress while the tangential stresses are continuous across the interface,

$$[\sigma_{ij} n_j]_{fs} = \tau \kappa n_i \tag{4.6a}$$
$$[\sigma_{ij} t_j]_{fs} = 0 \tag{4.6b}$$
$$[\sigma_{ij} s_j]_{fs} = 0, \tag{4.6c}$$

  where

$$\sigma_{ij} = -p\delta_{ij} + \nu(u_{i,j} + u_{j,i}), \tag{4.7}$$

  n_j is the normal to the interface, t_j and s_j are mutually orthogonal tangents to the interface, τ is the coefficient of surface tension and κ is the curvature.

A way to explicitly capture discrete jump conditions at the interface using level set technology is by the "Ghost Fluid" method of Fedkiw and collaborators [23, 41, 55]. In our case since we are not explicitly modeling one side of the interface, we do not need to use such methods. We neglect the shear stress conditions, eqns. 4.6b and 4.6c. Also, we neglect surface tension effects, reducing equation 4.6a to a statement that the pressure across the interface is continuous, i.e. $p_{liquid} = p_{air}$. In the examples presented in this dissertation, p_{air} is set to 0.

4.4 Computational Method

In this work we utilize the methodology described in [24] to solve for the velocity and pressure at each time step. In addition, the particle level set method is used to model the interface.

4.4.1 Finite Difference Discretization

A staggered MAC grid arrangement [31] is used to represent the velocity and pressure on a Cartesian computational grid. The pressure is stored at cell centers, while the components of the velocity are stored on the appropriate cell face as illustrated in figure 4.2. On a domain of size $(x_{min}, x_{max}) \times (y_{min}, y_{max}) \times (z_{min}, z_{max})$ with $(1, m) \times (1, n) \times (1, mn)$ grid points, Δx is given by $(x_{max} - x_{min})/m$ and $\vec{x}_{i,j,k} = (x_{min} + (i - .5)\,\Delta x, y_{min} + (j - .5)\,\Delta y, z_{min} + (k - .5)\,\Delta z)$.

An explicit first order in time fractional step method [44] utilizing the velocity projection method of Chorin [18] is used to advance the velocity and pressure fields in time. The convective term is discretized using a "Stable Fluid" semi-Lagrangian approach. An intermediate velocity field, $\vec{u}^*$ is calculated by

$$u^*_{i+1/2,j,k} = u^n(\vec{x}_{i+1/2,j,k} - \vec{u}^n_{i+1/2,j,k}\,\Delta t) \tag{4.8a}$$

$$v^*_{i,j+1/2,k} = v^n(\vec{x}_{i,j+1/2,k} - \vec{u}^n_{i,j+1/2,k}\,\Delta t) - g\Delta t \tag{4.8b}$$

$$w^*_{i,j,k+1/2} = w^n(\vec{x}_{i,j,k+1/2} - \vec{u}^n_{i,j,k+1/2}\,\Delta t), \tag{4.8c}$$

where g is the gravitational constant, $9.8m/s^2$. Trilinear interpolation is used to obtain values of the components of $\vec{u}$ which do not lie on grid points.

The new liquid velocity $\vec{u}^{n+1}$ is defined by

$$\frac{u^{n+1}_{i+1/2,j,k} - u^{*}_{i+1/2,j,k}}{\Delta t} + \frac{p^{n+1/2}_{i+1,j,k} - p^{n+1/2}_{i,j,k}}{\rho} = 0 \tag{4.9a}$$

$$\frac{v^{n+1}_{i,j+1/2,k} - v^{*}_{i,j+1/2,k}}{\Delta t} + \frac{p^{n+1/2}_{i,j+1,k} - p^{n+1/2}_{i,j,k}}{\rho} = 0 \tag{4.9b}$$

$$\frac{w^{n+1}_{i,j,k+1/2} - w^{*}_{i,j,k+1/2}}{\Delta t} + \frac{p^{n+1/2}_{i,j,k+1} - p^{n+1/2}_{i,j,k}}{\rho} = 0. \tag{4.9c}$$

Imposing the incompressibility constraint of equation 4.2 on $\vec{u}^{n+1}$, results in

$$\frac{\nabla \cdot \vec{u}^{*}}{\Delta t} = \nabla \cdot \left(\frac{\nabla p^{n+1/2}}{\rho} \right). \tag{4.10}$$

Written in component form, we obtain the following equation for $p_{i,j,k}$ at the $n+1/2$ time level,

$$p_{i+1,j,k} + p_{i,j+1,k} + p_{i,j,k+1} - 6p_{i,j,k} + p_{i-1,j,k} + p_{i,j-1,k} + p_{i,j,k-1} = \rho \frac{\Delta x}{\Delta t} D_{i,j,k} \tag{4.11}$$

assuming $\Delta x = \Delta y = \Delta z$. $D_{i,j,k}$ is the numerical divergence of the velocity defined as

$$D_{i,j,k} = u^{*}_{i+1/2,j,k} - u^{*}_{i-1/2,j,k} + v^{*}_{i,j+1/2,k} - v^{*}_{i,j-1/2,k} + w^{*}_{i,j,k+1/2} - w^{*}_{i,j,k-1/2}. \tag{4.12}$$

From equation 4.11 we can calculate the pressure, $p^{n+1/2}$, needed to ensure that the velocity is divergence-free at the $n+1$ time level. Since the system described by 4.11 is symmetric and positive definite (as long as there is at least one surface cell in the computational domain which slightly modifies the system as discussed below), we use an efficient Preconditioned Conjugate Gradient (PCG) as discussed in Golub and VanLoan [28] to determine $p^{n+1/2}_{i,j,k}$.

4.4.2 Velocity Extrapolation Near Free Surface

The presence of the free surface introduces some additional computational issues, especially in the treatment of equations 4.11 and 4.12. Due to our modeling assumptions, we apply the results of the above calculations only in cells which contain liquid. Cells with $\phi_{i,j,k} \leq 0$ at the center are determined to contain liquid. Surface cells are those which contain the $\phi = 0$ isocontour. In cells which have $\phi_{i,j,k} > 0$, we impose a Dirichlet boundary condition and define the pressure to be 0. This condition modifies the left-hand side of equation 4.11 by setting to zero any off-diagonal pressure terms in cells which have $\phi_{i\pm1,j\pm1,k\pm1} > 0$. The diagonal term is set to the number of neighboring liquid cells. The imposition of this boundary condition at cell centers and not at the exact location of the free surface introduces some error into the simulation, consequently degrading the calculation to first order accuracy near the interface. The accumulation of this error over time can degrade the accuracy of a simulation. In order to apply the pressure condition at the actual location of the free surface, an irregular finite difference stencil can be used as discussed in [12]. However, use of this more complicated stencil for the purposes of animation appears to be unnecessary as the results presented later in this chapter indicate.

A variety of methods have been used to computationally treat the calculation of the divergence of the velocity field on the interface. Velocities on the faces of surface cells which are adjacent to non-liquid cells will need to be determined even though these velocities may not lie within the liquid and are not explicitly modeled. A commonly used condition [31, 6, 25] is to set the undetermined velocities so that $D_{i,j,k} = 0$ is satisfied. Unfortunately, there are 64 distinct velocity configurations which need to be accounted for in three dimensions, not including the possibilities resulting from the presence of objects in the liquid or of walls at the boundaries. A less than rigorous analysis of all the possibilities can lead to the introduction of non-physical asymmetries into a simulation. For example, a detailed analysis of the computational velocity boundary conditions resulting from enforcing $D_{i,j,k} = 0$ at the free surface [15] showed that the velocity boundary conditions in the popular SMAC method [6] contained such an asymmetry. On the other hand Chan and Street [12] did not enforce $D_{i,j,k} = 0$ at the free surface since the free surface boundary

conditions discussed in section 4.3.2 do not place any conditions on $D_{i,j,k}$. Rather, they extrapolated the velocities from the liquid into the air using a Gregory-Newton backward interpolation formula in order to obtain a higher order accurate calculation of the velocity of the free surface. Even in highly viscous flows, faithful adherence of the simulation to the stress-free boundary conditions, eqns. 4.6a, 4.6b, and 4.6c is important in order to obtain *physically accurate* results [35, 56].

We choose to take a new approach to setting the unmodeled, but computationally required velocities, that takes advantage of the geometrical information contained in the level set function used to describe the free surface. We smoothly extrapolate the fluid velocities in the normal direction to the interface from inside the liquid. While this technique of extrapolating the velocity of the interface smoothly over the entire domain was first introduced to the level set community by Adalsteinsson and Sethian [2], its application to a free surface calculation is new. To calculate the extrapolated velocity, $\vec{u}_{ext} = (u_{ext}, v_{ext}, w_{ext})$, away from the interface we solve to steady state

$$\frac{\partial u_{ext}}{\partial \tau} + \vec{N} \cdot \nabla u_{ext} = 0 \tag{4.13a}$$

$$\frac{\partial v_{ext}}{\partial \tau} + \vec{N} \cdot \nabla v_{ext} = 0 \tag{4.13b}$$

$$\frac{\partial w_{ext}}{\partial \tau} + \vec{N} \cdot \nabla w_{ext} = 0, \tag{4.13c}$$

where τ is a fictitious time. The above equations are solved in band of 5 grid cells thick near the interface where $\phi > 0$. Since we have signed distance information to the free surface for the entire computational domain, $\vec{N}$ is given by $\nabla\phi$. At steady state we note that $\nabla\phi \cdot \nabla\{u_{ext}, v_{ext}, w_{ext}\} = 0$. This condition satisfies $D_{i,j,k} = 0$ at the free surface in the limit as the grid spacing approaches zero, since the divergence-free velocities are propagated unchanged in the normal direction across the interface. Also, since the update of the extrapolated variables occurs in only one direction outward from the interface, a fast $O(n \log n)$ marching technique [1] can be used to update $\vec{u}_{ext}$.

Use of this velocity extrapolation technique allows us to obtain a physically plausible velocity field in regions where we do not explicitly model the liquid. Besides providing for a reasonable way to calculate $D_{i,j,k}$ at the free surface, we can utilize the extrapolated velocity field for other purposes. Since we are using the particle level set method to model the interface, the existence of particles in the unmodeled "air" side of the interface requires that we have a reasonable velocity field in this region in order to move the particles. These particles are typically in a band a couple of grid cells thick about the interface, so having the capability to smoothly extrapolate velocities more than one grid cell away from the interface is crucial. Also, when using a semi-Lagrangian technique to update the velocity field inside the liquid near the interface, the flow characteristics may look back into the $\phi > 0$ region near the interface in order to determine which velocities to use in the update.

4.4.3 Particle Level Set Interface Treatment

We utilize the particle level set method as described in chapter 2 to model the interface. A dimension by dimension discretization of

$$\phi_t + \vec{u} \cdot \nabla \phi = 0 \tag{4.14}$$

using a fifth order accurate H-J WENO scheme is used along with a first order accurate forward Euler update in time. The particles are updated in time with a first order accurate forward Euler method which uses the velocities at time level n, i.e.

$$\vec{x}_p^{n+1} = \vec{x}_p^n + \vec{u}^n(\vec{x}_p^n). \tag{4.15}$$

Trilinear interpolation is used to determine the velocity of each particle.

For the examples shown in section 4.5 we perform a particle reseeding step every 20 frames. This reseeding is performed in order to maintain a reasonable distribution of particles about the entire fluid interface. This is necessary for the error correction step of the particle level set method to be effective. 64 particles per cell are used at all reseeding steps.

4.4.4 Boundaries

All of our calculations are performed in a computational domain which is open on the air at the top ($j = n$). We maintain a 3 grid cell thick band of ghost cells around the computational domain to assist in the semi-Lagrangian update of the velocity near the boundaries. For the level set we reflect the value of ϕ across the front, back, left, right, and bottom boundaries,

$$\phi_{1-l,j,k} = \phi_{l,j,k}, \quad \phi_{m+l,j,k} = \phi_{m-(l-1),j,k}, \tag{4.16a}$$

$$\phi_{i,j,1-l} = \phi_{i,j,l}, \quad \phi_{i,j,mn+l} = \phi_{i,j,mn-(l-1)}, \tag{4.16b}$$

$$\phi_{i,1-l,k} = \phi_{i,l,k}, \tag{4.16c}$$

where $l = \{1, 2, 3\}, i \in (1, m), j \in (1, n), k \in (1, mn)$. We wish to ensure that "air" or $\phi > 0$ is always above the computational domain at the $j = n$ boundary. For this boundary we use constant extrapolation if $\phi_{i,n,k} > 0$, else we set $\phi_{i,n+l,k} = \Delta y, l = \{1, 2, 3\}$ in the case of a liquid source at the top of the domain.

For each component of the velocity we implement the computational equivalents to the boundary conditions expressed by equations 4.3 and 4.4. For the top of the computational domain, we impose a constant extrapolation boundary condition. For example, the boundary conditions for u are

$$u_{1-l,j,k} = -u_{1+l,j,k}, \quad u_{m+l,j,k} = -u_{m-l,j,k}, \tag{4.17a}$$

$$u_{i,1-l,k} = u_{i,l,k}, \quad u_{i,n+l,k} = u_{i,n,k}, \tag{4.17b}$$

$$u_{i,j,1-l} = u_{i,j,l}, \quad u_{i,j,mn+l} = u_{i,j,mn-(l-1)}, \tag{4.17c}$$

where $l = \{1, 2, 3\}, i \in (1, m), j \in (1, n), k \in (1, mn)$. Similar boundary conditions apply for the v and w components of $\vec{u}$.

Particles which happen to cross one of the computational boundaries are placed back within the computational domain within a user defined ϵ of the boundary they crossed. Positive "air" particles which move beyond the top of the computational domain are deleted.

4.4.5 Time Step Calculation

Use of a semi-Lagrangian method to calculate the intermediate velocity $\vec{u}^*$ allows one to take a larger time step than that allowed according to the CFL time step restriction for an explicit time discretization of the convective portion of equation 4.1,

$$\Delta t \left(\frac{|u|_{max}}{\Delta x} + \frac{|v|_{max}}{\Delta y} + \frac{|w|_{max}}{\Delta z} \right) \leq 1, \tag{4.18}$$

where $|u|_{max}, |v|_{max}$, and $|w|_{max}$ are the maximum magnitudes of the velocities. While the use of as large as possible a time step is useful in an animation environment since it provides for fast turnaround times, using such a large time step to update the motion of the interface according to equation 4.14 can cause a visually disturbing loss (or gain) of mass to occur. Instead, we use the time step subcycling scheme proposed in [24] to evolve the particles and level set function associated with the particle level set method in time according to a plausible CFL condition,

$$\Delta t_{levelset} = .5 \ \min \left(\frac{\Delta x}{|u|_{max}}, \frac{\Delta y}{|v|_{max}}, \frac{\Delta z}{|w|_{max}} \right). \tag{4.19}$$

The liquid velocity field, $\vec{u}$, is updated at a rate given by

$$\Delta t_{liquid} = 4.9 \, \Delta t_{levelset}. \tag{4.20}$$

Between the liquid velocity updates, the particles and level set function are evolved forward in time according the most recently computed velocity field.

4.4.6 Overall Computational Cycle

After initializing the level set function and the particles, the computation of the liquid and the free surface proceeds as follows. Data from the simulation is written out to a file at time intervals given by a user defined frame rate. Before each liquid update, the level set and particles are integrated with a time step given by equation 4.19 as many times as necessary in order to reach Δt_{liquid}. A fractional-step procedure is used in which a preliminary velocity field is calculated from equations 4.8a - 4.8c.

Then, the pressure is calculated according to equation 4.10 with the appropriate boundary conditions applied. A PCG method as discussed in [28] is used to solve the system. The method terminates after achieving a relative tolerance of 10^{-8} or after 20 iterations are performed. We have found this is sufficient to have the simulation maintain the appearance of a liquid. This pressure is then applied to previously calculated velocity field in order to satisfy the incompressibility condition of a liquid. The newly calculated fluid velocities are then smoothly extrapolated outward from the fluid into the air near the interface. This cycle repeats until the time to write the current frame to file is reached. A schematic of the computational steps performed per frame is given by figure 4.3.

4.5 Examples

4.5.1 Rendering

The renderings of the animations of water being poured into a glass and the splash generated by the impact of a ball in a tank of water were performed by Dr. Stephen Marschner using a physically based Monte Carlo ray tracer capable of handling all types of illumination using photon maps and irradiance caching [38]. A geometry primitive that intersects rays with the implicit surface directly by solving for the root of the signed distance along the ray was created for use by the rendering system. Depending on the accuracy required by a particular scene we use either a trilinear or a tricubic filter [50] to reconstruct ϕ. The normal is computed using trilinearly interpolated central differences for the trilinear surface, or simply using the derivative of the reconstructed tricubic surface.

The properties of ϕ have two advantages in the rendering context. First, intersecting a ray with the surface is much more efficient than it would be for an isosurface of a general function. The signed distance function provides a lower bound on the distance to the intersection along the ray, allowing us to take large steps when the current point is far from the surface. Second, it is easy to provide for motion blur in the standard distribution ray tracing framework. To compute the surface at an

intermediate time between two frames we simply interpolate between the two signed distance volumes and use the same intersection algorithm unchanged. For the small motions that occur between frames the special properties of ϕ are not significantly compromised.

The breaking wave results are rendered by Neil Herzinger and Willi Geiger of Industrial Light + Magic using a proprietary renderer.

All frames and movies generated from the following calculations can be found on the CD-ROM included with this dissertation.

4.5.2 Pouring A Glass of Water

Figures 4.5 and 4.6 show the high degree of complexity in the water surface. Note the liveliness of the surface of the water when it is initially being poured. The ability to maintain the visually pleasing thin sheets of water during the turbulent mixing phase is a consequence of our new method. We do not lose any of the fine detail of the air pockets formed, since we model both sides of the water surface. The calculation was performed on a Cartesian grid of size $55 \times 120 \times 55$ and grid spacing of $0.01m$ in each direction. The glass was modeled on the grid as a cylinder of radius 25 grid cells and the major axis located at (0.275, 0.0, 0.275) and running parallel to the y-axis, with the grid points outside the cylinder treated as an object which does not permit the fluid to penetrate it. In order to avoid any difficulties in interpolating ϕ near the edge of the cylinder, a constant extrapolation of ϕ away from the cylinder using the value of ϕ at a location of $(0.0001\,\Delta x)$ from the surface inside the cylinder was used. A full slip velocity boundary along the walls of the cylinder was used. The glass was modeled as smooth and clear in order to highlight the action of the water being poured into the glass. The water inlet was modeled as a cylinder of radius 0.075 and height of .03 placed at (.275, 1.17, .275) with the major axis running parallel to the y-axis. An injection velocity of $(-1.0, -1.5, 0.0)m/s$ was used. To update the grid points inside the source, the velocity inside cylinder is fixed, along with the value of ϕ being set to Δx and a Neumann boundary condition being enforced inside the source. In order to ensure that particles are seeded inside the source a particle reseeding step

restricted to a region about the source was performed at the end of each particle level set subcycling step. A frame rate of 72 frames per second was used. The simulation time was 9 seconds, with the source turned off after 6 seconds. The computational cost was approximately 8 minutes per frame on a 2GHz Pentium IV processor with 2GB of RAM.

The scene used to render our result contains just a simple cylindrical glass, the simulated water surface, and a few texture mapped polygons for the background. Illumination comes from a physically based sky model and two area sources. Because water only reflects and refracts other objects, the scene including the sky is very important to the appearance. The glass and the water together create three dielectric interfaces: glass-air, water-air, and air-water, so the inside surface of the glass has two sets of material properties depending on whether it is inside or outside the implicitly defined surface (which is easy to determine by checking the sign of ϕ). The illumination in the shadow of the glass is provided by a photon map, and illumination from the sky on diffuse surfaces in the scene is computed using Monte Carlo integration. Motion blur was included for these renderings. The rendering time for the glass was approximately 15 minutes per frame.

4.5.3 Splash Generated From Ball Impact

In this example we simulate the impact and resulting splash from a heavy ball being thrown into a tank of water. This simulation was performed to illustrate the ability of our method to interact with animated objects in the scene to provide a point of comparison with an identically performed calculation by Foster and Fedkiw [24]. The size of the tank is $1.4 \times 1.1 \times 0.9m$. The simulation was performed using a computational domain of size $140 \times 110 \times 90$. The tank was initially filled with water to a depth of .4 m. A procedurally animated ball of size $.1m$ was made to fly into the pool at a velocity of $(-4.5, -4.5, 0.)m/s$. Once the ball has reached the bottom of the tank, it ceases to move. The ball affects the dynamics of the water, but the water does not affect the motion of the ball in any way. In order to obtain more realistic behavior, the ball could be treated as a rigid body which dynamically interacts with

the liquid. We enforce a tangential slip boundary condition around the ball and a normal velocity boundary condition which prevents water from flowing into the object. The level set function, ϕ, is set to $+\Delta x$ and any particles which enter the object are deleted.

The results of the simulation are seen in figures 4.9 and 4.10. The ball enters the water and generates an initial splash sheet. A large amount of air is entrained by the ball as it enters the water due to the non-physical, animation of the ball motion in the water, causing a very large secondary splash sheet to be formed. The particle level set method is able to resolve these thin splash sheets. A frame rate of 72 frames per second was used. The overall simulation encompassed 5.6 seconds. A comparison between the use of the hybrid liquid volume model of Foster and Fedkiw and the particle level set method is seen in figures 4.7 and 4.8. The lack of particles in the "air", $\phi > 0$, region is clearly evident in figure 4.7. The interface in the Foster and Fedkiw result is suffering from an excessive amount of diffusion into the air region as evidenced due to the formation of a hump backed shaped region in front of the splash sheet. The hybrid volume model does not use any outside particle to correct for this effect. The particle level set method on the other hand is able to maintain the visually pleasing thin splash sheet without an excessive amount of diffusion of the interface.

4.5.4 Breaking Wave

We have performed a breaking wave calculation in a numerical wave tank as shown in figures 4.13 and 4.14. To begin to model this phenomenon, we needed to chose an initial condition for the wave. We used the solution for a solitary wave of finite amplitude propagating without shape change [65]. The initial velocities u and v in

the x and y directions respectively and surface height η are given by:

$$u = \sqrt{gd}\frac{H}{d}\,\mathrm{sech}^2\left[\sqrt{\frac{3H}{4d^3}}x\right] \tag{4.21}$$

$$v = \sqrt{3gd}\left(\frac{H}{d}\right)^{3/2}\frac{y}{d}\,\mathrm{sech}^2\left[\sqrt{\frac{3H}{4d^3}}x\right]\tanh\left[\sqrt{\frac{3H}{4d^3}}x\right] \tag{4.22}$$

$$\eta = d + H\,\mathrm{sech}^2\left[\sqrt{\frac{3H}{4d^3}}x\right], \tag{4.23}$$

where g is the gravitational constant $9.8m/s^2$. For our simulations, we set $H = 7$ and $d = 10$. We used the same initial conditions in three spatial dimensions, replicating the two dimensional initial conditions along the z-axis.

Next, we introduced a model of a sloping beach in order to cause the propagating pulse to form a breaking wave. We performed a variety of two dimensional tests to determine the best underwater shelf geometry to generate a visually pleasing breaking wave. Figure 4.11 is a sequence of frames from one of the two dimensional tests we ran with the same x-y cross section as in our 3D example. We found this prototyping technique to be a fast and easy way to explore breaking wave behavior in a fraction of the time it would take to run a fully three dimensional test case.

After determining the best submerged shelf geometry to generate a breaking wave, we generated a slight tilt in the geometry in order to induce a curl in the break of the wave and enhance the three dimensional look. A sketch of the shelf geometry used in our three dimensional calculations is shown in figure 4.12. An incline of slope 1:7 rises up from the sea bottom to a depth of 2 m below the surface of the water. Instead of allowing the incline to go all the way to the surface we chose to have it flatten out at this depth in order to illustrate the splash up effects after the initial breaking of the wave.

Next we ran a fully three dimensional simulation, the results of which can be seen in figures 4.13 and 4.14. The simulation was run on a computational grid of size $540 \times 75 \times 120$ and of dimensions $180 \times 25 \times 40m$. A frame rate of 72 frames per second was used. 12 seconds of simulated wave behavior were calculated. The

wave has the intended curling effect. The formation of a tube of air is clearly seen after the wave splashes down, with the "air" particles maintaining the tube even after the wave begins a secondary splash up. We observe some solely three dimensional effects including the fingering of the breaking wave. The fine detail features seen on the surface of the ocean surface, including the appearance of capillary waves and foam were generated through the use of procedural displacement textures and matte texture maps respectively. In order to simulate these details one would need to use a finer computational grid along with a different velocity advection scheme than the diffusive semi-Lagrangian method used here. However, for the purposes of computer graphics we can use other methods besides physically-based animation techniques in order to obtain plausible looking fine details to place on the wave. The goal of this simulation was to show that the hard-to-animate bulk motion of the interface can be obtained by using relatively simple algorithms from the computational fluid dynamics community. The computational cost of this simulation was approximately 13 minutes per frame.

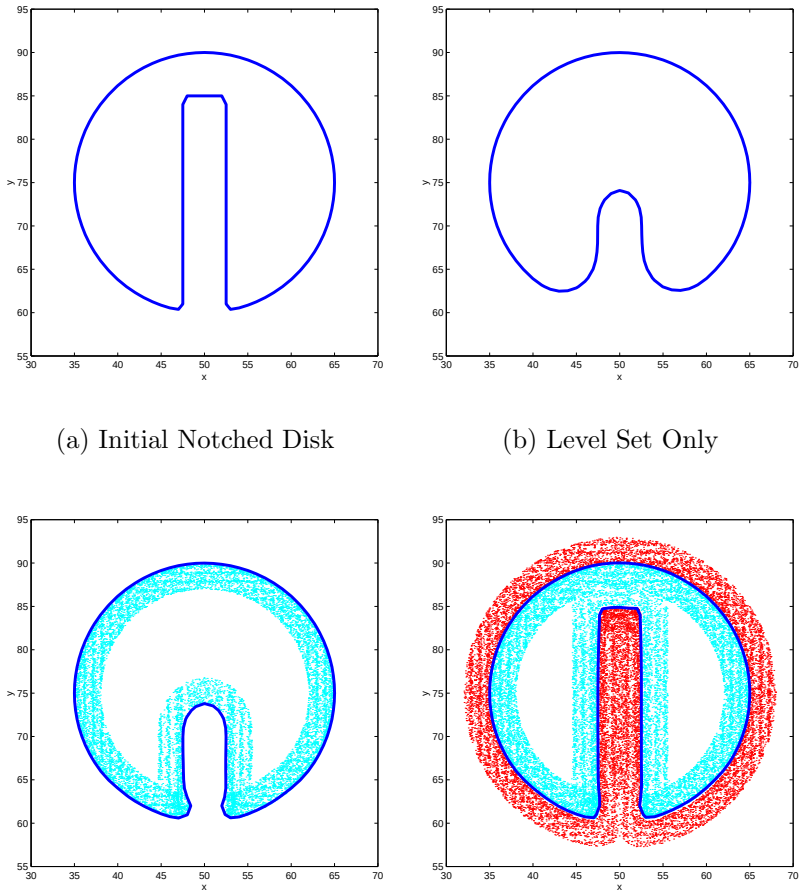

(a) Initial Notched Disk

(b) Level Set Only

(c) Hybrid Volume Model

(d) Particle Level Set

Figure 4.1: Comparison of Hybrid Volume Model and the Particle Level Set method for one rotation of Zalesak's Disk

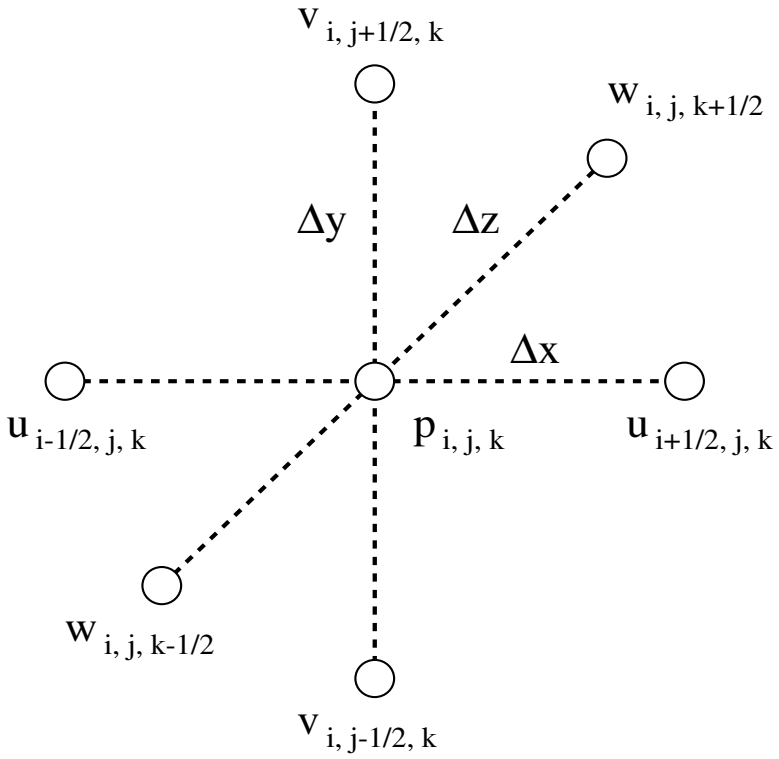

Figure 4.2: Velocity-Pressure (MAC) staggered grid arrangement

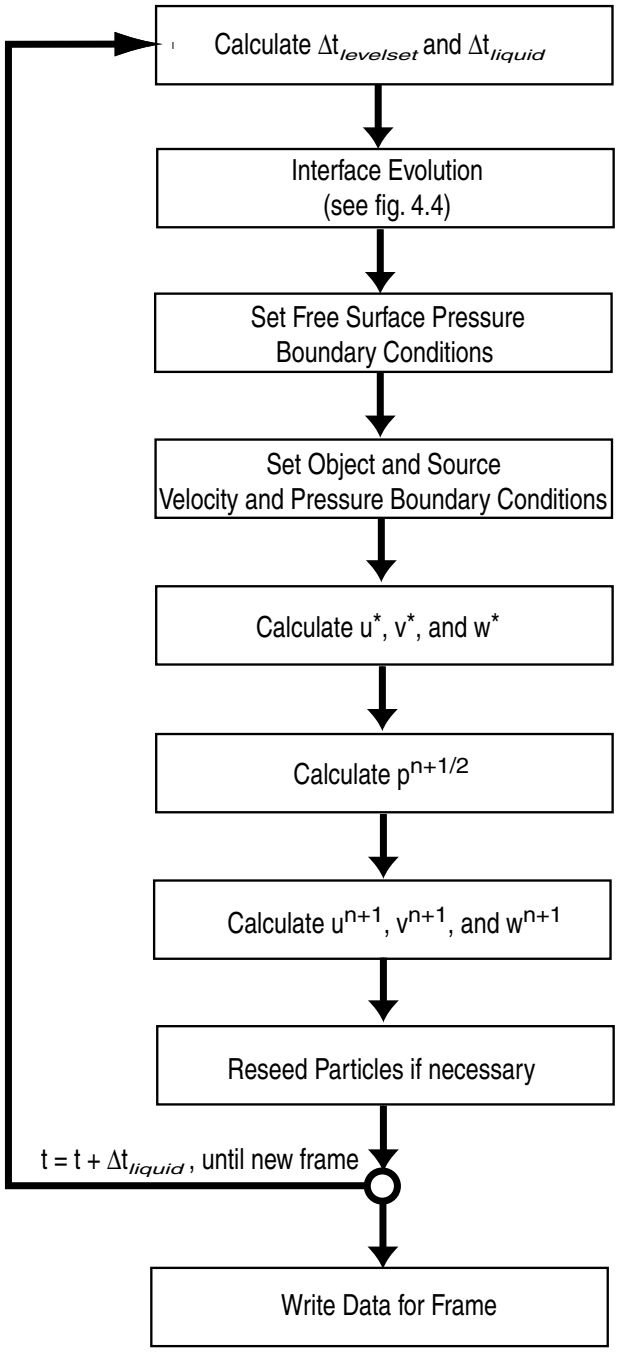

Figure 4.3: Free Surface Overall Computational Cycle

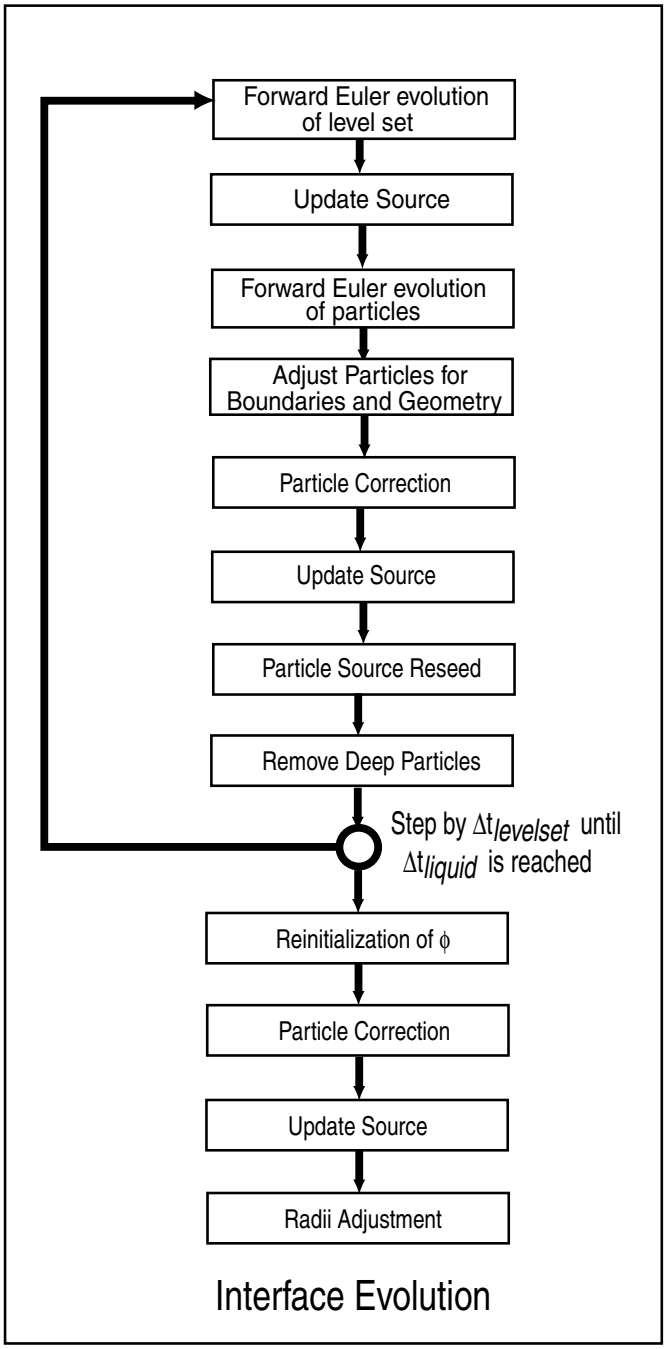

Figure 4.4: Free Surface Interface Evolution

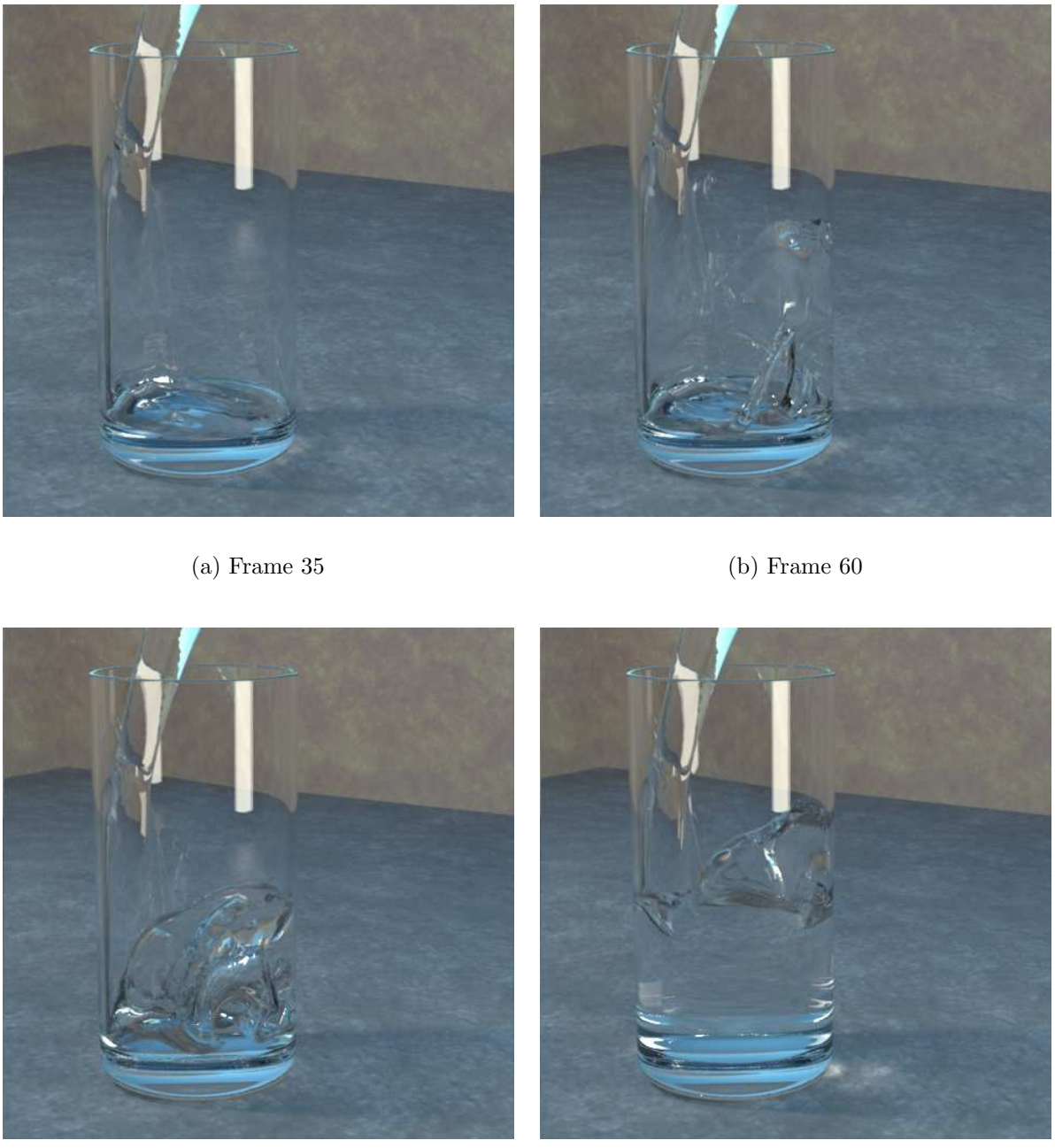

(a) Frame 35

(b) Frame 60

(c) Frame 100

(d) Frame 300

Figure 4.5: Water being poured into a clear, cylindrical glass.

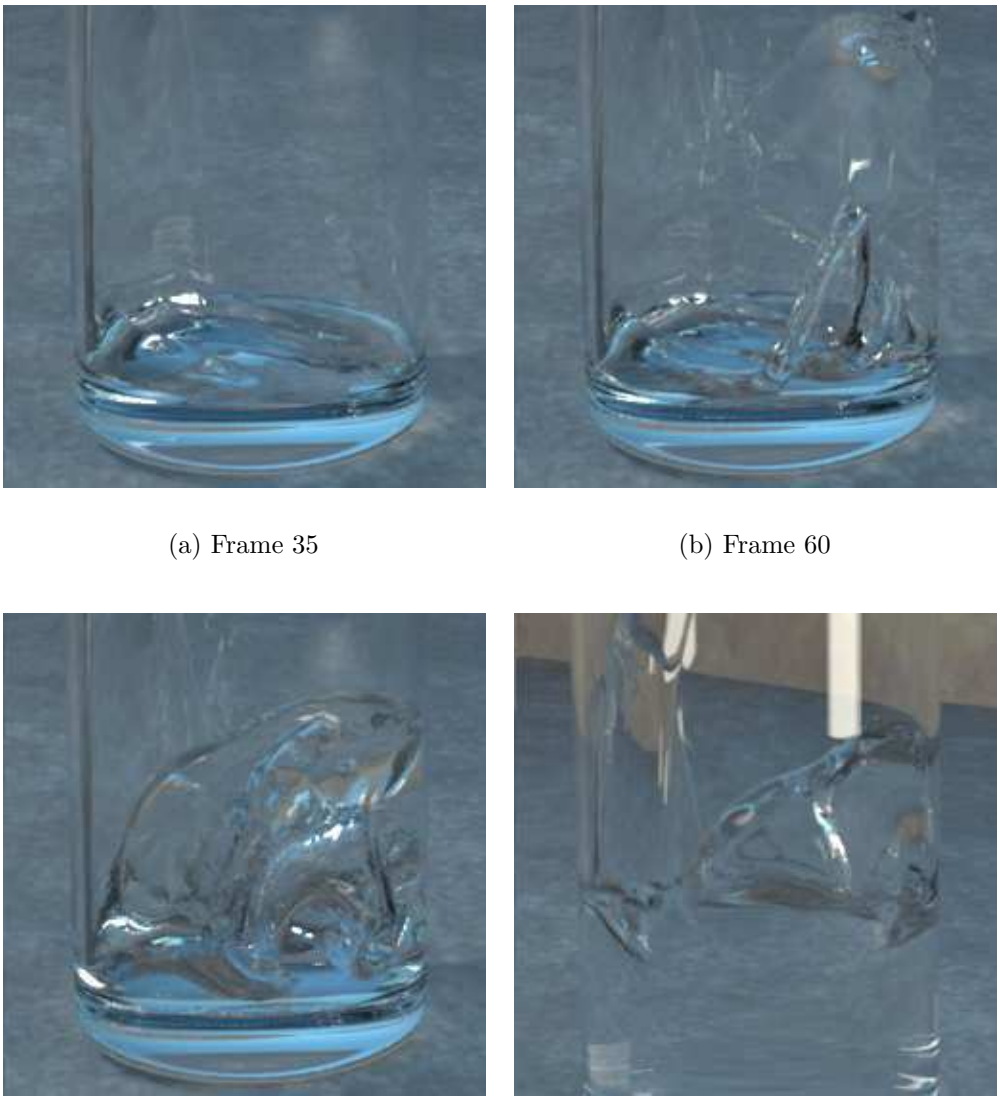

(a) Frame 35

(b) Frame 60

(c) Frame 100

(d) Frame 300

Figure 4.6: Closeup of figure 4.5. Our method makes possible the fine detail seen in the turbulent mixing of the water and air.

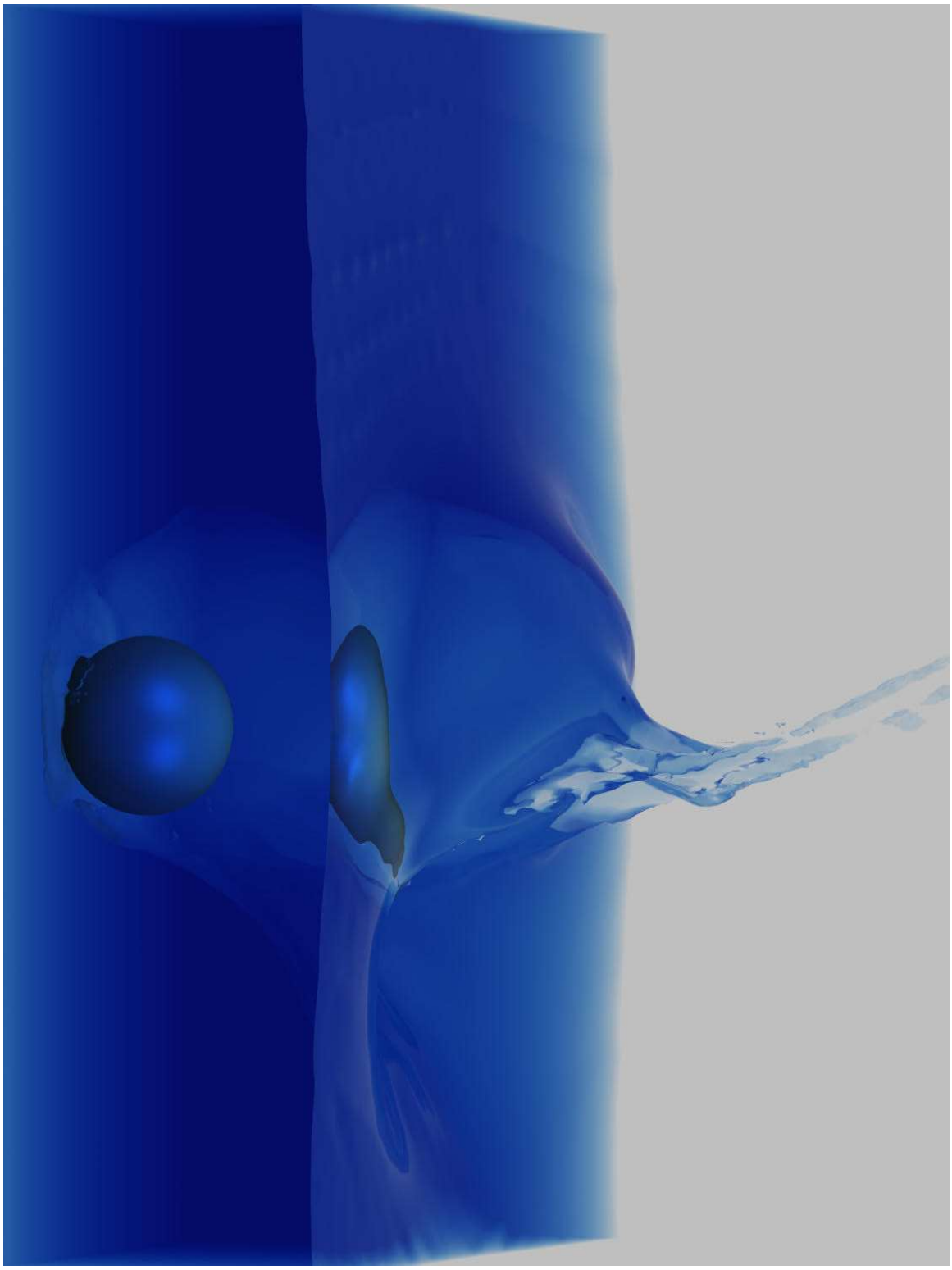

Figure 4.7: Ball thrown into a tank of water. Hybrid Volume Model result.

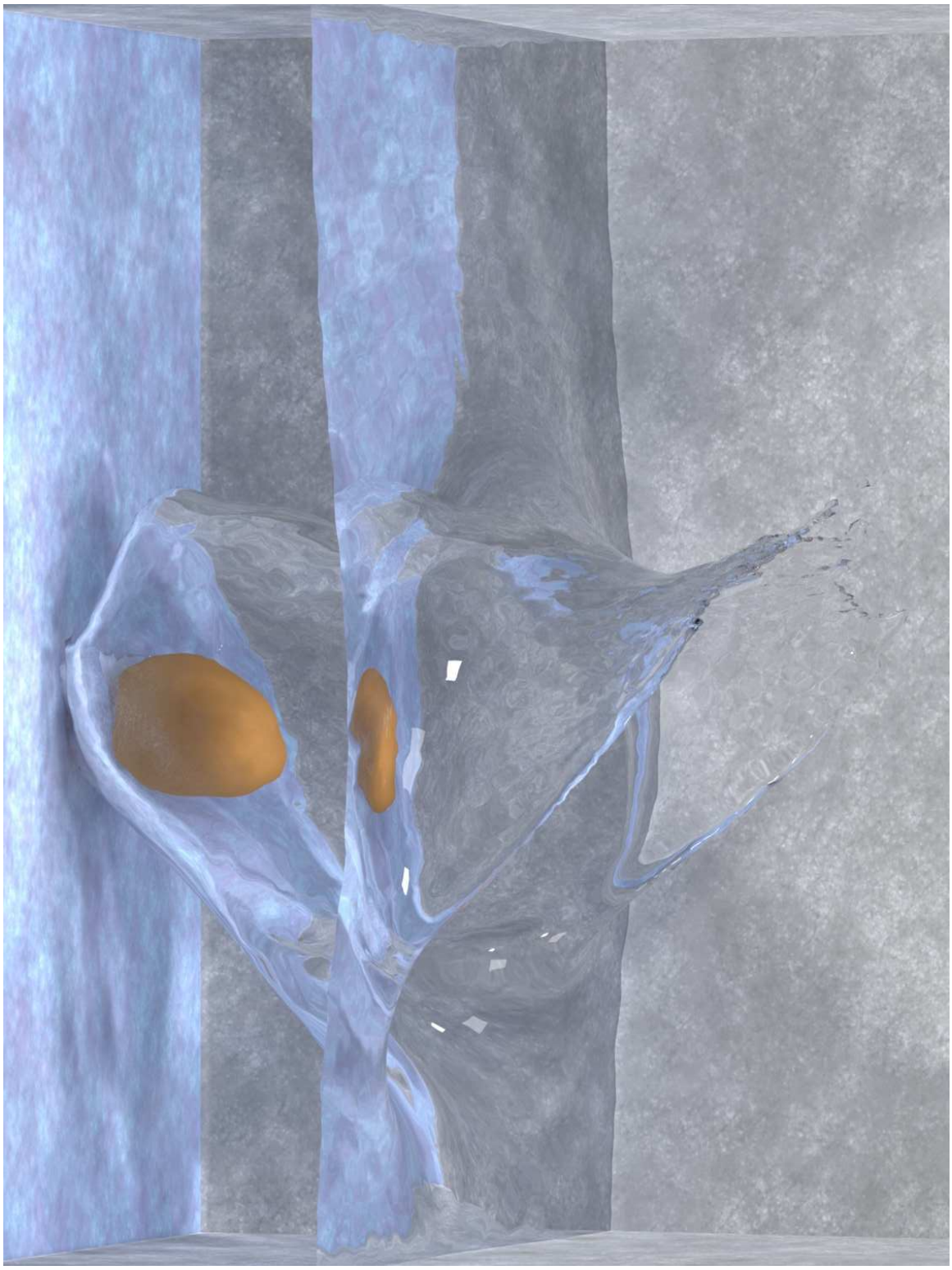

Figure 4.8: Ball thrown into a tank of water. Particle Level Set result.

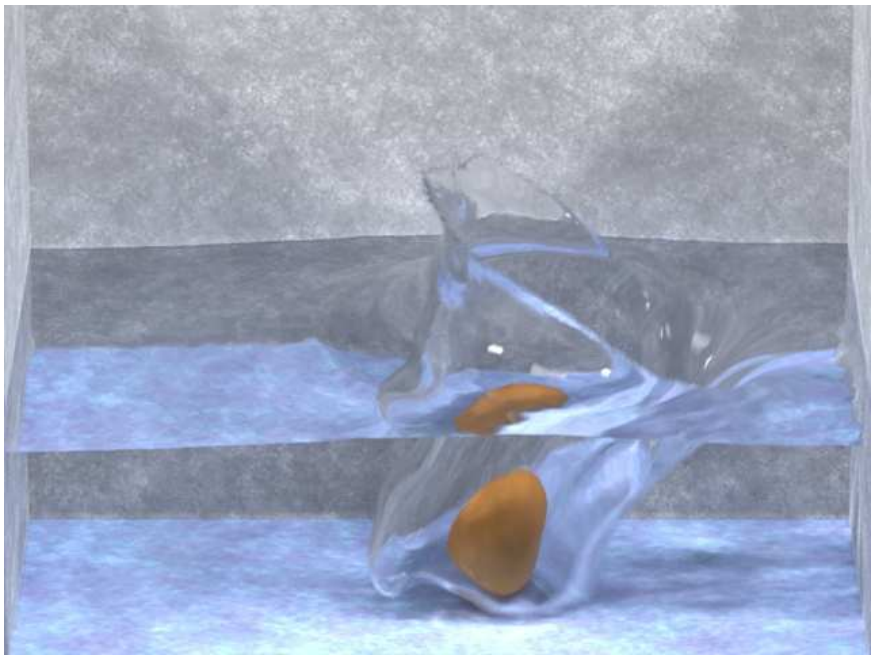

(a) Frame 19

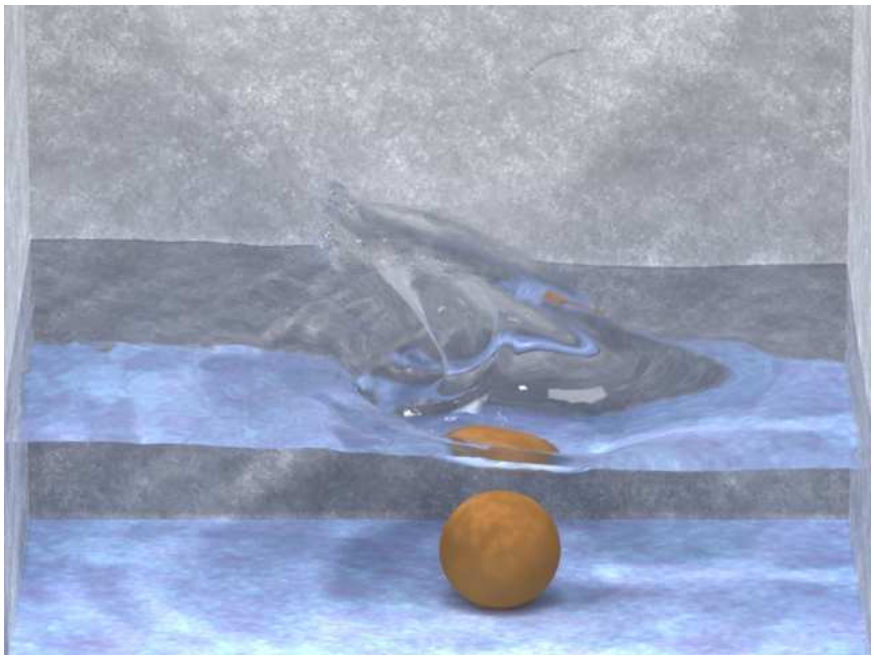

(b) Frame 36

Figure 4.9: Ball thrown into a tank of water. Formation of intial and secondary splash sheets.

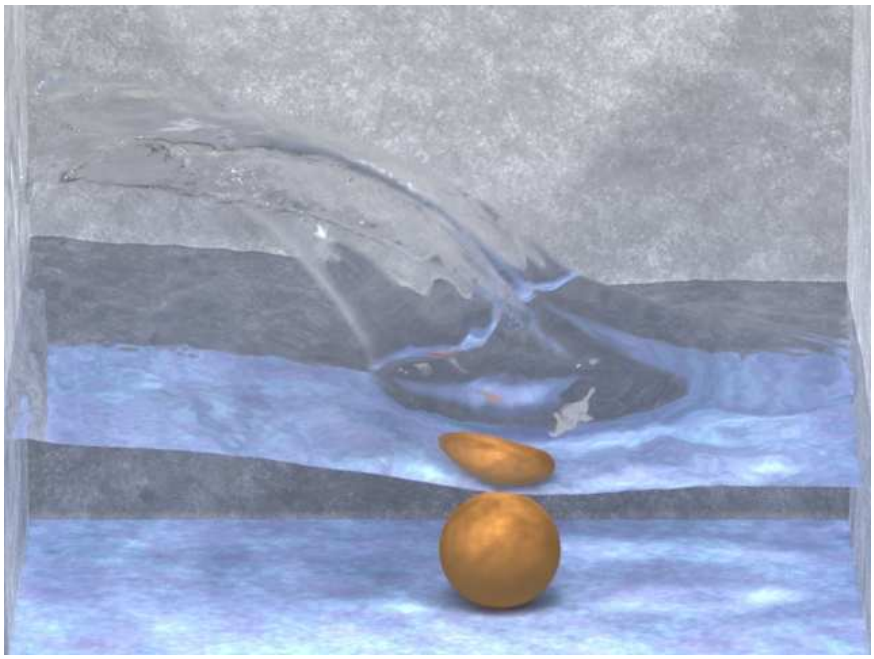

(a) Frame 52

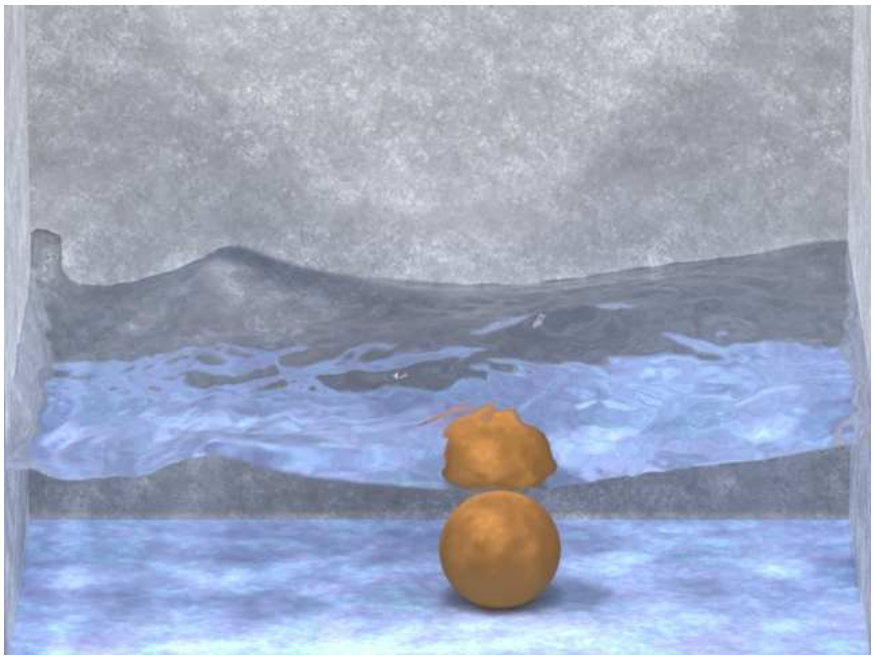

(b) Frame 100

Figure 4.10: Ball thrown into a tank of water. Secondary splash sheet and resulting surface.

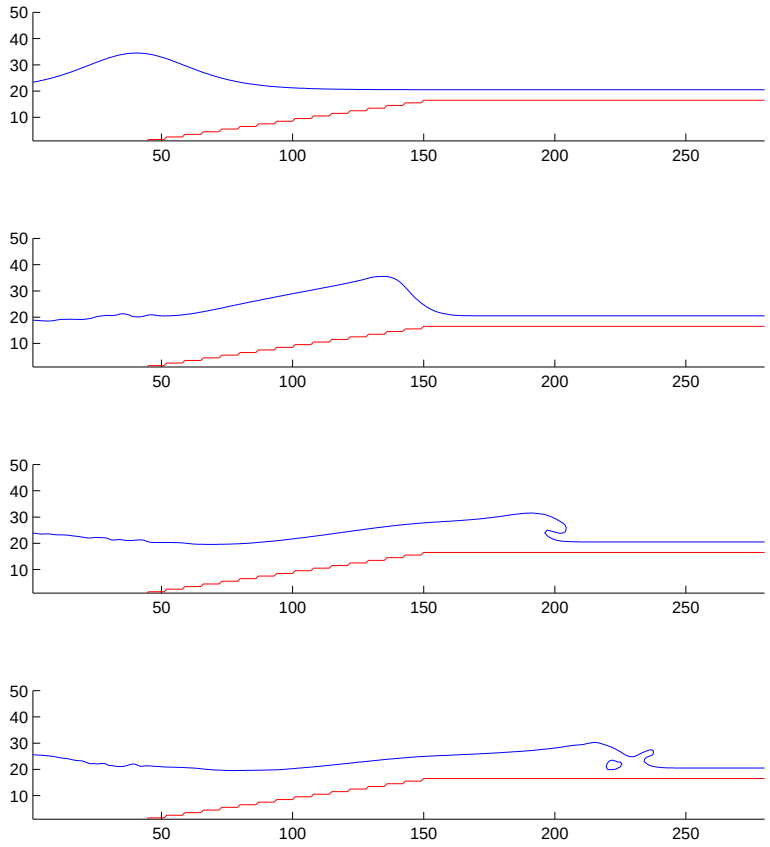

Figure 4.11: Two Dimensional Breaking Wave

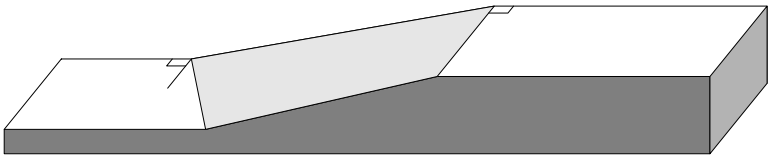

Figure 4.12: Submerged Shelf

(a) Frame 80

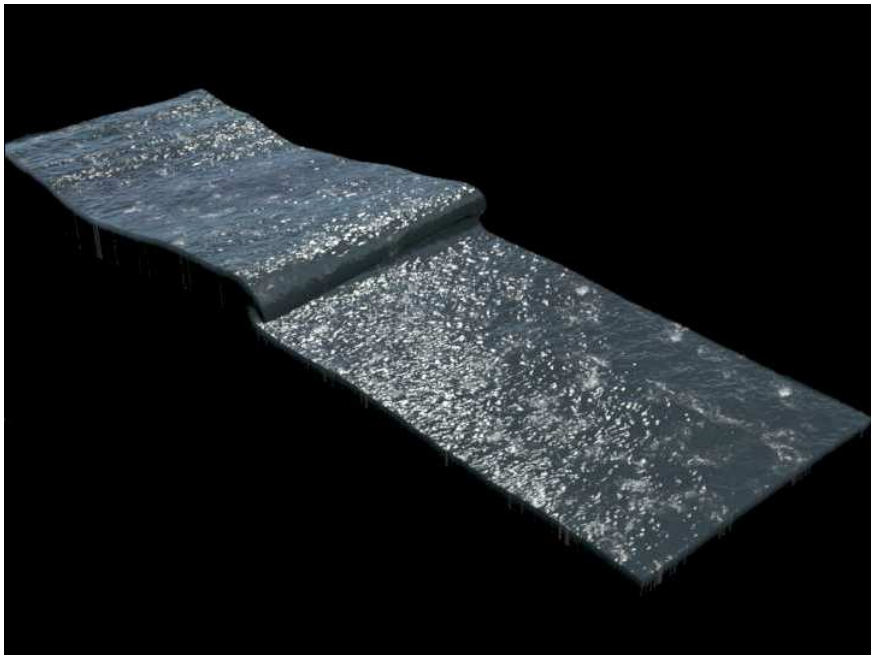

(b) Frame 130

Figure 4.13: View of wave breaking on a submerged shelf. Note the ability to properly model the initial breaking phase of the wave.

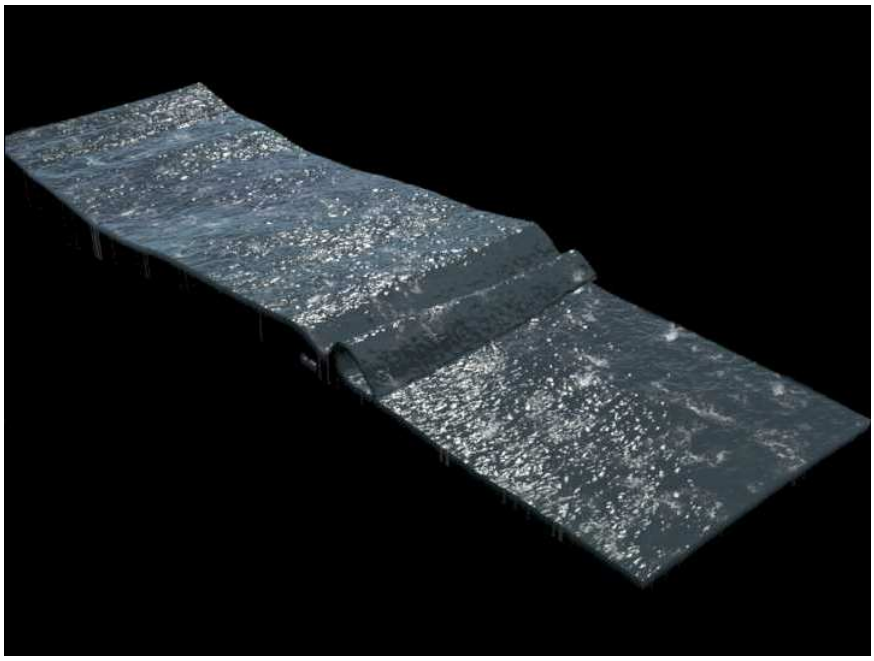

(a) Frame 170

(b) Frame 288

Figure 4.14: View of wave breaking on a submerged shelf. Note the ability to properly model the secondary splash up and bore creation phase.

Chapter 5

Conclusions and Future Directions

We have proposed a new numerical method which combines the best aspects of Eulerian front capturing schemes and Lagrangian front tracking methods for improved mass conservation. Level set methods are used to capture the smooth part of the interface, but suffer an excessive amount of mass loss in under-resolved regions. This prevents the resolution of thin filaments and regions of high curvature. To counteract this problem, characteristic information is provided by massless marker particles. Escaped massless marker particles are used to correct the mass loss in the level set function. The method otherwise maintains the desirable geometric properties of level set methods along with the ease and simplicity of implementation. As seen in the examples contained in chapter 3, the "particle level set method" compares favorably with volume of fluid methods with regards to conservation of mass and purely Lagrangian schemes for interface resolution.

While we add particles in a band near the interface, other strategies could be adopted. For example, it is obvious that particles are only needed in regions of high curvature and restricting particles to these regions would speed up the method significantly. Concerning speed, it is interesting to compare this method to adaptive meshing, for example as in [81]. A significant advantage of particle methods is that they avoid the small time step restriction dictated by the small cells produced by adaptive meshing. Also, the data structures are simpler than for cell based adaptive meshing, and the particle method can be applied more locally than patch based

adaptive meshing.

We combined the "particle level set method" with a liquid free surface simulation code in order to gauge the effectiveness of this method in maintaining a topologically complex liquid interface in a computer animation environment. In order to use this method, we took advantage of a well known tool in the level set community, velocity extrapolation, in order to obtain a smooth, divergence free velocity field in the "air" region near the interface. We performed three different animations, the pouring of a glass of water, the splash formed due to the impact of a ball thrown into a tank of water, and of a three dimensional, breaking surface wave. While breaking wave calculations have been performed for some time in the computational fluid dynamics community, see [48], this is the first time in an animation context that a breaking wave calculation has been performed. The "particle level set method" combined with velocity extrapolation near the interface appears to be a robust interface technique in order to perform liquid animations on the coarse computational grids commonly used in a production environment.

Future work includes using the "particle level set method" in order to calculate enhanced resolution simulations of a variety of free surface flows including capillary jet break up, the turbulent mixing resulting from plunging water waves, and the motion of bubbles and drops. Extending the method to simulate the formation and evolution of interfaces comprised of multiple immiscible fluids (such as those flows consisting of air, oil, and water) [98, 99] would be challenging and of practical engineering interest. An economically important application of the method would be the robust simulation of the turbulent flow along the hull and behind the stern of a ship. There exists complex physical processes including the breaking water waves, spray formation, and free-surface turbulence. All of these phenomena contribute to the resistance that a ship feels while moving through a body of water. Examples of ongoing work in this area can be found in [22, 82]. By being able to experiment on a computer using an accurate and robust Cartesian based method like the "particle level set method", different hull designs can be tested to see which produce the least drag.

While it has been demonstrated that the "particle level set method" is an effective method to track contact discontinuities, one of the applications which motivated

the creation of the method is the multidimensional aircraft collision avoidance calculations performed by Mitchell and Tomlin [89, 54]. In this application where the dimensionality of the PDE used is commonly higher than any flow calculation, a level set method is used to determine the safe sets for aircraft control systems in order to avoid collision. Due to the large number of degrees of freedom, the computational grid used is fairly coarse and, as a result, controlling the amount of numerical diffusion is of great concern. Particle methods have been used to sample a finite number of states, which provides a very crude approximation of the overall safe set. Since the governing equation for the evolution of the level set in this application is a discontinuous Hamilton-Jacobi equation instead of an advection equation, this equation admits not only contact discontinuities but also shocks and rarefactions. As illustrated in chapter 1, particles are unable to capture the proper viscosity solution in the presence of shocks in the flow field. One future goal is to modify the particle level set method in order to make the error correction step a two-way process, in the case of a contact discontinuity the particles propagate error information to the level set and vice versa in the case of shocks.

Bibliography

[1] Adalsteinsson, D. and Sethian, J., *A Fast Level Set Method for Propagating Interfaces*, J. Comp. Phys. 118, 269–277 (1995).

[2] Adalsteinsson, D. and Sethian, J., *The Fast Construction of Extension Velocities in Level Set Methods*, J. Comp. Phys. 148, 2–22 (1999).

[3] Agresar, G., Linderman, J., Tryggvason, G. and Powell, K., *An Adaptive, Cartesian, Front-Tracking Method for the Motion, Deformation and Adhesion of Circulating Cells*, J. Comp. Phys. 143, 346–380 (1998).

[4] Aleinov, I., Puckett, E. and Sussman, M., *Formation of Droplets in Microscale Jetting Devices*, in *Proceedings of the Third ASME/JSME Joint Fluids Engineering Conference, FEDSM99-7106*, 1999.

[5] Amsden, A., *Numerical Calculation of Surface Waves: A Modified ZUNI Code with Surface Particles and Partial Cells*, Technical Report LA-5146, Los Alamos Scientific Laboratory (1973).

[6] Amsden, A. and Harlow, F., *The SMAC Method: A Numerical Technique for Calculating Incompressible Fluid Flows*, Technical Report LA–4370, Los Alamos Scientific Laboratory (1970).

[7] Baker, G. R., Meiron, D. I. and Orszag, S. A., *Generalized vortex methods for free-surface flow problems*, J. Fluid Mech. 123, 477–501 (1982).

[8] Bell, J., Colella, P. and Glaz, H., *A Second-Order Projection Method for the Incompressible Navier-Stokes Equations*, J. Comp. Phys. 85, 257–283 (1989).

[9] Briggs, W. L., *A Multigrid Tutorial*, SIAM, Philadelphia, PA, 1987.

[10] Caiden, R., Fedkiw, R. and Anderson, C., *A Numerical Method For Two-Phase Flow Consisting of Separate Compressible and Incompressible Regions*, J. Comp. Phys. 166, 1–27 (2001).

[11] Cerne, G., Petelin, S. and Tiselj, I., *Coupling of the Interface Tracking and the Two-Fluid Models for the Simulation of Incompressible Two-Phase Flow*, J. Comp. Phys. 171, 776–804 (2001).

[12] Chan, R. K.-C. and Street, R. L., *A Computer Study of Finite-Amplitude Water Waves*, J. Comp. Phys. 6, 68–94 (1970).

[13] Chang, Y., Hou, T., Merriman, B. and Osher, S., *A Level Set Formulation of Eulerian Inteface Capturing Methods for Incompressible Fluid Flows*, J. Comp. Phys. 124, 449–464 (1996).

[14] Chen, J. and Lobo, N., *Toward Interactive-Rate Simulation of Fluids with Moving Obstacles Using the Navier-Stokes Equations*, Computer Graphics and Image Processing 57, 107–116 (1994).

[15] Chen, S., Johnson, D. and Raad, P., *Velocity Boundary Conditions for the Simulation of Free Surface Fluid Flow*, J. Comp. Phys. 116, 262–276 (1995).

[16] Chen, S., Johnson, D., Raad, P. and Fadda, D., *The Surface Marker and Micro Cell Method*, Int. J. for Num. Meth. in Fluids 25, 749–778 (1997).

[17] Chopp, D. L., *Some Improvements of the Fast Marching Method*, SIAM J. Sci. Comput. 23, 230–244 (2002).

[18] Chorin, A. J., *Numerical Solution of the Navier-Stokes Equations*, Math. Comp. 22, 745–762 (1968).

[19] Cottet, G.-H. and Koumoutsakos, P. D., *Vortex Methods*, Cambridge Univ. Press, Cambridge, UK, 2000.

[20] Courant, R., Issacson, E. and Rees, M., *On the Solution of Nonlinear Hyperbolic Differential Equations by Finite Differences*, Comm. Pure and Applied Math 5, 243–255 (1952).

[21] DeBar, R., *A Method in Two-D Eulerian Hydrodynamics*, Technical Report UCID-19683, Lawrence Livermore National Laboratory (1974).

[22] Farmer, J., Martinelli, L. and Jameson, A., *Fast Multigrid Method for Solving Incompressible Hydrodynamic Problems with Free Surfaces*, AIAA Jounral 32, 1175–1182 (1994).

[23] Fedkiw, R. P., Aslam, T., Merriman, B. and Osher, S., *A Non-oscillatory Eulerian Approach to Interfaces in Multimaterial Flows (The Ghost Fluid Method)*, J. Comp. Phys. 152, 457–492 (1999).

[24] Foster, N. and Fedkiw, R., *Practical Animation of Liquids*, in Fiume, E., ed., *Proceedings of SIGGRAPH 2001*, Computer Graphics Proceedings, Annual Conference Series, pp. 23–30, ACM, ACM Press / ACM SIGGRAPH, 2001.

[25] Foster, N. and Metaxas, D., *Realistic Animation of Liquids*, Graphical Models and Image Processing 58, 471–483 (1996).

[26] Fournier, A. and Reeves, W. T., *A Simple Model of Ocean Waves*, in *Computer Graphics (Proceedings of SIGGRAPH 86), 20(4)*, pp. 75–84, ACM, 1986.

[27] Glassner, A., *Principles of Digital Image Synthesis*, Morgan Kaufmann Publishers, Inc., San Francisco, CA, 1995.

[28] Golub, G. H. and Loan, C. F. V., *Matrix Computations*, Johns Hopkins University Press, Baltimore, MD, 1996, 3rd edition.

[29] Grilli, S. T., Guyenne, P. and Dias, F., *A fully non-linear model for three-dimensional overturning waves over an arbitrary bottom*, Int. J. for Num. Meth. in Fluids 35, 829–867 (2001).

[30] Harlow, F., Shannon, J. and Welch, J., *THE MAC METHOD: A Computing Technique for Solving Viscous, Incompressible, Transient Fluid-Flow Problems Involving Free Surfaces*, Technical Report LA-3425, Los Alamos Scientific Laboratory (1965).

[31] Harlow, F. and Welch, J., *Numerical Calculation of Time-Dependent Viscous Incompressible Flow of Fluid with Free Surface*, Phys. Fluids 8, 2182–2189 (1965).

[32] Helmsen, J., *A Comparison of Three-Dimensional Photolithography Development Methods*, Ph.D. thesis, U.C. Berkeley (1994).

[33] Hiltzik, M. A. and Pham, A., *Synthetic Actors Guild*, Los Angeles Times (2001), may 8, 2001, natl. ed. : A1+.

[34] Hirt, C. and Nichols, B., *Volume of Fluid (VOF) Method for the Dynamics of Free Boundaries*, J. Comp. Phys. 39, 201–225 (1981).

[35] Hirt, C. and Shannon, J., *Free-Surface Stress Conditions for Incompressible-Flow Calculations*, J. Comp. Phys. 2, 403–411 (1968).

[36] Hou, T., Lowengrub, J. and Shelley, M., *Boundary Integral Methods for Multicomponent Fluids and Multiphase Materials*, J. Comp. Phys. 169, 302–362 (2001).

[37] Hou, T. Y., *Numerical Solutions to Free Boundary Problems*, Acta Numerica pp. 335–415 (1995).

[38] Jensen, H. W., *Realistic Image Synthesis Using Photon Maps*, A K Peters, 2001.

[39] Jiang, G.-S. and Peng, D., *Weighted ENO Schemes for Hamilton-Jacobi Equations*, SIAM J. Sci. Comput. 21, 2126–2143 (2000).

[40] Johnsgard, H., *A Numerical Model for Run-Up of Breaking Waves*, Int. J. for Num. Meth. in Fluids 31, 1321–1331 (1999).

[41] Kang, M., Fedkiw, R. and Liu, X.-D., *A Boundary Condition Capturing Method for Multiphase Incompressible Flow*, J. Sci. Comput. 15, 323–360 (2000).

[42] Kass, M. and Miller, G., *Rapid, Stable Fluid Dynamics for Computer Graphics*, in *Computer Graphics (Proceedings of SIGGRAPH 90)*, volume 24, pp. 49–57, ACM, 1990.

[43] Kim, I. and Sirignano, W. A., *Three-dimensional wave distortion and disintegration of thin planar liquid sheets*, J. Fluid Mech. 410, 147–183 (2000).

[44] Kim, J. and Moin, P., *Application of a fractional-step method to incompressible Navier-Stokes equations*, J. Comp. Phys. 59, 308–323 (1985).

[45] Lafaurie, B., Nardone, C., Scardovelli, R., Zaleski, S. and Zanetti, G., *Modelling Merging and Fragmentation in Multiphase Flows with SURFER*, J. Comp. Phys. 113, 134–147 (1994).

[46] Lapenta, G. and Brackbill, J., *Dynamic and Selective Control of the Number of Particles in Kinetic Plama Simulations*, J. Comp. Phys. 115, 213–227 (1994).

[47] Leveque, R., *High-Resolution Conservative Algorithms For Advection In Incompressible Flow*, SIAM J. Numer. Anal. 33, 627–665 (1996).

[48] Longuet-Higgins, M. and Cokelet, E., *The deformation of steep surface waves on water. I. A numerical method of computation*, Proc. R. Soc. London Ser. A 350, 1–26 (1976).

[49] Mansour, N. and Lundgren, T., *Satellite formation in capillary jet breakup*, Phys. Fluids A 2, 1141–1144 (1990).

[50] Marschner, S. and Lobb, R., *An Evaluation of Reconstruction Filters for Volume Rendering*, in *Proceedings of Visualization 94*, pp. 100–107, IEEE Comput. Soc. Press, 1994.

[51] Masten, G., Watterberg, P. and Mareda, I., *Fourier Synthesis of Ocean Scenes*, IEEE Computer Graphics and Application 7, 16–23 (1987).

[52] McDonald, A., *Accuracy of Multiply-Upstream, Semi-Lagrangian Advective Schemes*, Monthly Weather Review 112, 1267–1275 (1982).

[53] Miller, G. and Pearce, A., *Globular Dynamics: A Connected Particle System for Animating Viscous Fluids*, Computers and Graphics 13(3), 305–309 (1989).

[54] Mitchell, I. and Tomlin, C., *Level Set Methods for Computation in Hybrid Systems*, in Krogh, B. and Lynch, N., eds., *Hybrid Systems: Computation and Control*, pp. 310–323, Springer Verlag, 2000.

[55] Nguyen, D. Q., Fedkiw, R. P. and Kang, M., *A Boundary Condition Capturing Method for Incompressible Flame Discontinuities*, J. Comp. Phys. 172, 71–98 (2001).

[56] Nichols, B. and Hirt, C., *Improved Free Surface Boundary Conditions for Numerical Incompressible-flow Calculations*, J. Comp. Phys. 8, 434–448 (1971).

[57] O'Brien, J. and Hodgins, J., *Dynamic Simulation of Splashing Fluids*, in *Proceedings of Computer Animation 95*, pp. 198–205, 1995.

[58] Osher, S. and Fedkiw, R., *Level Set Methods: An Overview and Some Recent Results*, J. Comp. Phys. 169, 463–502 (2001).

[59] Osher, S. and Fedkiw, R., *The Level Set Method and Dynamic Implicit Surfaces*, Springer-Verlag, New York, 2002.

[60] Osher, S. and Sethian, J., *Fronts Propagating with Curvature Dependent Speed: Algorithms Based On Hamiliton-Jacobi Formulations*, J. Comp. Phys. 79, 12–49 (1988).

[61] Peachey, D. R., *Modeling Waves and Surf*, in *Computer Graphics (Proceedings of SIGGRAPH 86), 20(4)*, pp. 65–74, ACM, 1986.

[62] Peng, D., Merriman, B., Osher, S., Zhao, H.-K. and Kang, M., *A PDE-Based Fast Local Level Set Method*, J. Comp. Phys. 155, 410–438 (1999).

[63] Puckett, E., Almgren, A., Bell, J., Marcus, D. and Rider, W., *A High-Order Projection Method for Tracking Fluid Interfaces in Variable Density Incompressible Flows*, J. Comp. Phys. 130, 269–282 (1997).

[64] Raad, P., Chen, S. and Johnson, D., *The Introduction of Micro Cells to Treat Pressure in Free Surface Fluid Flow Problems*, J. Fluids Eng. 117, 683–690 (1995).

[65] Radovitzky, R. and Ortiz, M., *Lagrangian Finite Element Analysis of Newtonian Fluid Flows*, Int. J. Numer. Meth. Engng. 43, 607–619 (1998).

[66] Rider, W. and Kothe, D., *A Marker Particle Method for Interface Tracking*, in Dwyer, H., ed., *Proceedings of the Sixth International Symposium on Computational Fluid Dynamics*, pp. 976–981, 1995.

[67] Rider, W. and Kothe, D., *Stretching and Tearing Interface Tracking Methods*, in *12th AIAA CFD Conference*, 95–1717, AIAA, 1995.

[68] Rider, W. and Kothe, D., *Reconstructing Volume Tracking*, J. Comp. Phys. 141, 112–152 (1998).

[69] Schachter, B., *Long Crested Wave Models*, Computer Graphics and Image Processing 12, 187–201 (1980).

[70] Sethian, J., *Curvature and the Evolution of Fronts*, Comm. Math. Phys. 101, 487–499 (1985).

[71] Sethian, J., *Numerical Methods for Propagating Fronts*, in Concus, P. and Finn, R., eds., *Variational Methods for Free Surface Interfaces*, Springer-Verlag, 1987.

[72] Sethian, J., *A Fast Marching Level Set Method for Monotonically Advancing Fronts*, Proc. Natl. Acad. Sci. 93, 1591–1595 (1996).

[73] Sethian, J., *Fast Marching Methods*, SIAM Rev. 41, 199–235 (1999).

[74] Sethian, J., *Level Set Methods and Fast Marching Methods*, Cambridge University Press, 1999.

[75] Sethian, J., *Evolution, Implementation, and Application of Level Set and Fast Marching Methods for Advancing Fronts*, J. Comp. Phys. 169, 503–555 (2001).

[76] Shu, C. and Osher, S., *Efficient Implementation of Essentially Non-Oscillatory Shock Capturing Schemes*, J. Comp. Phys. 77, 439–471 (1988).

[77] Smolarkiewicz, P., *The Multi-Dimensional Crowley Advection Scheme*, Monthly Weather Review 110, 1968–1983 (1982).

[78] Stam, J., *Stable Fluids*, in *Proceedings of SIGGRAPH 99*, Computer Graphics Proceedings, Annual Conference Series, pp. 121–128, ACM, ACM SIGGRAPH / Addison Wesley Longman, 1999.

[79] Staniforth, A. and Côté, J., *Semi-Lagrangian Integration Schemes for Atmospheric Models - A Review*, Montly Weather Review 119, 2206–2223 (1991).

[80] Sussmam, M. and Puckett, E., *A Coupled Level Set and Volume-of-Fluid Method for Computing 3D and Axisymmetric Incompressible Two-Phase Flows*, J. Comp. Phys. 162, 301–337 (2000).

[81] Sussman, M., Almgren, A., Bell, J., Colella, P., Howell, L. and Welcome, M., *An Adaptive Level Set Approach for Incompressible Two-Phase Flows*, J. Comp. Phys. 148, 81–124 (1999).

[82] Sussman, M. and Dommermuth, D., *The Numerical Simulation of Ship Waves Using Cartesian Grid Methods*, in *Twenty-Third Symposium on Naval Hydrodynamics*, pp. 762–779, 2001.

[83] Sussman, M. and Fatemi, E., *An Efficient, Interface-Preserving Level Set Redistancing Algorithm and Its Application to Interfacial Incompressible Fluid Flow*, SIAM J. Sci. Comput. 20, 1165–1191 (1999).

[84] Sussman, M., Fatemi, E., Smereka, P. and Osher, S., *An Improved Level Set Method for Incompressible Two-Phase Flows*, Comput. and Fluids 27, 663–680 (1998).

[85] Sussman, M., Smereka, P. and Osher, S., *A Level Set Approach for Computing Solutions to Incompressible Two-Phase Flow*, J. Comp. Phys. 114, 146–159 (1994).

[86] Terzopoulos, D., Platt, J. and Fleischer, K., *Heating and melting deformable models (From goop to glop)*, in *Graphics Interface '89*, pp. 219–226, 1989.

[87] Tomé, M., Filho, A., Cuminato, J., Mangiavacchi, N. and McKee, S., *GENSMAC3D: a numerical method for solving unsteady three-dimensional free surface flows*, Int. J. for Num. Meth. in Fluids 37, 747–796 (2001).

[88] Tomé, M., McKee, S., Barratt, L., Jarvis, D. and Patrick, A., *An Experimental and Numerical Investigation of Container Filling With Viscous Liquids*, Int. J. for Num. Meth. in Fluids 31, 1333–1353 (1999).

[89] Tomlin, C., Mitchell, I. and Ghosh, R., *Safety Verification of Conflict Resolution Manoeuvres*, IEEE Trans. Intell. Transp. Syst. 2, 110–120 (2001).

[90] Torres, D. and Brackbill, J., *The Point-Set Method: Front Tracking without Connectivity*, J. Comp. Phys. 165, 620–644 (2000).

[91] Tryggvason, G., Bunner, B., Esmaeeli, A., Juric, D., Al-Rawahi, N., Tauber, W., Han, J., Nas, S. and Jan, Y.-J., *A Front-Tracking Method for the Computations of Multiphase Flow*, J. Comp. Phys. 169, 708–759 (2001).

[92] Unverdi, S.-O. and Tryggvason, G., *A Front-Tracking Method for Viscous, Incompressible, Multi-fluid Flows*, J. Comp. Phys. 100, 25–37 (1992).

[93] Williams, M., Kothe, D. and Puckett, E., *Approximating Interfacial Topologies with Applications for Interface Tracking Algorithms*, in *37th AIAA Aerospace Sciences Meeting*, AIAA 99–1076, 1999.

[94] Williams, M., Kothe, D. and Puckett, E., *Convergence and Accuracy of Kernal-Based Continuum Surface Tension Models*, in Shyy, W., ed., *Fluid Dynamics at Interfaces*, pp. 347–356, Cambridge University Press, 1999.

[95] Witting, P., *Computational Fluid Dynamics in a Traditional Animation Environment*, in *Proceedings of SIGGRAPH 99*, Computer Graphics Proceedings, Annual Conference Series, pp. 129–136, ACM, ACM SIGGRAPH / Addison Wesley Longman, 1999.

[96] Zalesak, S., *Fully Multidimensional Flux-Corrected Transport Algorithms for Fluids*, J. Comp. Phys. 31, 335–362 (1979).

[97] Zhang, Y., Yeo, K., Khoo, B. and Wang, C., *3D Jet Impact and Toroidal Bubbles*, J. Comp. Phys. 166, 336–360 (2001).

[98] Zhao, H.-K., Chan, T., Merriman, B. and Osher, S., *A Variational Level Set Approach to Multiphase Motion*, J. Comp. Phys. 127, 179–195 (1996).

[99] Zhao, H.-K., Merriman, B., Osher, S. and Wang, L., *Capturing the Behavior of Bubbles and Drops Using the Variational Level Set Approach*, J. Comp. Phys. 143, 495–518 (1998).